1986

Ultraviolet Variability and Mass Expulsion from R Aquarii

Menas Kafatos
Chapman University, kafatos@chapman.edu

A. G. Michalitsianos
NASA, Goddard Space Flight Center

J. M. Hollis
Blue Bay Research, Inc

Recommended Citation
Kafatos, M., Michalitsianos, A,G., Hollis, J,M. (1986) Ultraviolet Variability and Mass Expulsion from R Aquarii, *The Astrophysical Journal Supplement Series*, 62: 853-874. doi: 10.1086/191158

Ultraviolet Variability and Mass Expulsion from R Aquarii

THE ASTROPHYSICAL JOURNAL SUPPLEMENT SERIES, 62:853–874, 1986 December

ULTRAVIOLET VARIABILITY AND MASS EXPULSION FROM R AQUARII

M. KAFATOS[1]
Department of Physics, George Mason University, Fairfax, Virginia
AND
A. G. MICHALITSIANOS[1] AND J. M. HOLLIS[1]
Laboratory for Astronomy and Solar Physics, NASA/Goddard Space Flight Center, Greenbelt, Maryland
Received 1986 April 17; accepted 1986 May 29

ABSTRACT

Ultraviolet spectra obtained in the 1200–3200 Å range over the course of 4 yr with the *International Ultraviolet Explorer* (*IUE*) indicate that the extended nebular features which resemble a jet in the peculiar variable R Aquarii (M7e+pec) have increased in excitation in 1985. This is indicated by the appearance of He II λ1640 and N V λλ1238, 1240 in the jet features and is consistent with the detection of soft X-rays, as found with *EXOSAT* in 1985. We have analyzed the emission properties of the compact H II region that surrounds the unresolved binary, and those of the extended nebular jet, from the low-resolution *IUE* spectra which we obtained of these regions. In particular, the UV line intensities observed in the jet appear variable on a time scale of ~1.5 yr. A new accretion disk model is proposed that explains the kinematic and ionization properties of discrete components which comprise the jet emission nebulosity, the appearance of the jet in the 1980s, and morphology that uniquely characterizes the R Aquarii system at radio, optical, UV, and X-ray wavelengths.

Subject headings: nebulae: H II regions — stars: binaries — stars: emission-line — stars: individual — stars: mass loss — stars: symbiotic — ultraviolet: spectra

I. INTRODUCTION

This investigation is concerned with determining the near- and far-ultraviolet emission properties of the symbiotic variable R Aquarii and its jet, in context with the observed radio structure. The radio morphology which characterizes the jet has been completely determined by high spatial resolution observations acquired with the Very Large Array (VLA)[2] (Kafatos, Hollis, and Michalitsianos 1983; Hollis *et al.* 1986). In order to determine the excitation properties of the H II region which surrounds the binary system, as well as the emission features which comprise the jet, we have obtained ultraviolet spectra with the *International Ultraviolet Explorer* (*IUE*) over the course of 4 yr.

Previous *IUE* observations of R Aqr by Michalitsianos, Kafatos, and Hobbs (1980), Johnson (1980, 1982) and Michalitsianos and Kafatos (1982) support a binary model for this object. UV radiation from a hot subdwarf star and accretion disk photoionizes a compact H II nebula. The H II nebula engulfs the hot star and the 387 day period Mira variable. Previous *IUE* observations of R Aqr revealed the presence of moderate-excitation emission lines, which include C III], C IV, O III], O IV], Si III], Si IV, N III], and N IV]. Encircling the compact H II region is a filamentary oval nebula, which is ~2′ in extent, and oriented east-west in its major axis. The two intersecting arcs of the meniscus-shaped nebula are expanding with a velocity ~ 50–100 km s^{-1} (Baade 1944). Also, oriented nearly north-south, an inner nebula which subtends ~1′ appears to be perpendicular to the larger, outer, east-west structure.

In 1977 Wallerstein and Greenstein (1980) detected a "spike" or "jet" of nebular material extending ~6″ northeast from R Aqr. The jet appeared to be the brightest feature except for R Aqr itself in integrated light (Herbig 1980). Radio maps obtained in 1981 at the VLA in the "C antenna array" at 6 cm (limiting spatial resolution ~4″–5″) indicated that the optical emission was cospatial with extended radio structure (Sopka *et al.* 1982; Spergel, Giuliani, and Knapp 1983), at a position angle ~29°. Subsequent higher spatial resolution VLA radio maps obtained in 1982 at 6 cm (Kafatos, Hollis, and Michalitsianos 1983) resolved R Aqr into several discrete radio knots (features A and B; Fig. 1).

Recent high spatial resolution VLA observations of R Aqr have been obtained at 2, 6, and 20 cm (Hollis *et al.* 1985) and indicate that radio features A and B, which comprise the "jet," are cospatial with extended structure observed at optical wavelengths (Sol 1983; Mauron *et al.* 1985). Furthermore, the radio spectral index obtained for the central compact H II region suggests optically thick thermal radio emission, whereas the radio spectral index of feature B indicates optically thin thermal emission (Hollis *et al.* 1985). Solf and Ulrich (1985) obtained high-resolution optical echelle spectra of the inner north-south bipolar nebula, as well as the 2′ east-west meniscus-shaped outer nebula. A review summarizing the major properties of the jet, and the general nebulosity which uniquely characterizes R Aqr, is given by Michalitsianos (1984).

In order to spatially resolve the central system and determine whether any marked geometrical asymmetry exists at

[1]Guest Investigator, *International Ultraviolet Explorer* (*IUE*).
[2]The VLA is a facility of the National Radio Astronomy Observatory, which is operated by Associated Universities, Inc., under contract with the National Science Foundation.

greater resolution, VLA observations in the "A antenna array" at 2 cm (limiting resolution ~ 0".1) were recently obtained (Hollis *et al.* 1986). Unexpectedly, the central H II region divided into two additional components (Hollis *et al.* 1986). The brighter of the two radio components is designated C1, and the fainter C2. Determining which of the two new radio features, C1 or C2, corresponds to the position of the R Aqr binary is difficult, because the exact position of the Mira variable in the optical is not known with subarcsecond precision. For example, the difference between the SAO position (SAO 165849) and the HD catalog (HD 222800) is about 2". Here we assume that the stronger of the two newly found radio features, C1, corresponds to the position of the Mira hot subdwarf binary. At their respective distances from feature C1 (compact H II region), component C2 is 0".5, component A is 2".7, and component B is 6".5 away from the position of the binary.

It has been argued recently that the newly found radio/optical features in R Aqr do not exhibit significant proper motion, suggestive of a rapid flow of material. Accordingly, the term "jet" is not appropriate for R Aqr (cf. Solf and Ulrich 1985; Taylor, Seaquist, and Mattei 1986). However, Bridle and Perley (1984) note for extragalactic radio jets (with only one exception) that there is "no *direct* evidence for flow in any continuous extragalactic jet." Following Bridle and Perley (1984), we adopt three basic criteria which provide a working definition for jets:

1. "*At least four times as long as it is wide.*"—The most extended feature, B, which is approximately 6".5 distant from C1, and ~ 2".3 in its smallest dimension (see Fig. 8), yields a ratio of ~ 3, in rough agreement with this criterion.

2. "*Separable in high resolution from other extended structures.*"—The R Aqr jet is distinguished from the general extended nebulosity which characterizes the large-scale structure of the system, because features A, B, and C2, as well as the central compact H II region C1, emit at microwave and ultraviolet wavelengths. The surrounding and more extended east-west and north-south nebula emits mainly recombination lines, and is characterized generally by lower ionization species, with no detectable radio emission.

3. "*Aligned with the compact radio core where it is closest.*"—Features C2, A, and B lie at position angles 55°, 45°, and 29°, respectively. Their positions with respect to the compact H II region (C1) suggests a continuous curve, or arc, reminiscent of "bent" or "curved" tails seen in extragalactic radio jets.

Additionally, radio contours from 6 cm VLA maps indicate bipolar morphology, with features A and A′ suggesting jet and counterjet symmetry (Fig. 1). Accordingly, we adopt the term "jet" as applicable to radio/optical features of R Aqr.

Far-ultraviolet *IUE* spectra obtained of R Aqr over 4 years indicate that the jet features are steadily increasing in excitation. From our *IUE* observations in 1982, features A and B (Michalitsianos and Kafatos 1982) appeared lower in excitation compared with the central H II region. However, our 1985 *IUE* observations indicate that N V λλ1238, 1240 and He II λ1640 have intensified in the jet. These emission lines are weak or absent in the central compact H II region surrounding the binary. The appearance of these high-excitation lines suggests that the extended nebular jet features are continuing to increase in excitation, compared with the H II region, which appears nearly constant in excitation between 1982 and 1985. The detection of soft X-rays in the 0.25–1 keV range from R Aqr with *EXOSAT* (Baratta *et al.* 1985) is consistent with the appearance of N V and He II emission. Moreover, our *IUE* observations support the suggestion that X-rays are probably emitted primarily from the extended jet features, where we have observed the highest excitation lines in the far-ultraviolet.

We describe our *IUE* data on R Aqr and the jet/spike which were obtained over 4 yr. Analysis of these data has led to a new model for the formation of the jet, which can explain the ionization and kinematic properties of the radio/optical features.

II. OBSERVATIONS

Our *IUE* observing program is summarized in Table 1. UV observations in the SWP 1200–2000 Å and LWP/LWR 2000–3200 Å ranges were obtained in the large (10" × 20") aperture of *IUE*. The spatial extent of the jet has enabled us to isolate *IUE* spectra of the features that comprise (1) the jet and (2) the central compact H II region. We used 6 cm VLA radio maps (Kafatos, Hollis, and Michalitsianos 1983) as a means of accurately positioning the *IUE* entrance aperture. In Figure 1, *IUE* echelle spectra of the compact H II region (SWP 24811) and the jet (features A and B) (SWP 24810) are shown, with corresponding positions of the large aperture. In order to ensure that offset pointings for features A and B were repeated exactly for each epoch, the same guide star was used for tracking (fine error sensor [FES] position: $X = 992$, $Y = 406$; FES counts ~ 44 in slow track). The dates of observation correspond approximately to the same spacecraft orientation in roll (~ 325°) and yaw as shown in Figure 1. Thus, spectra at different epochs can be intercompared. Owing to uncertainties in extinction (Kaler 1981; Whitelock *et al.* 1983), the spectra shown are not corrected for reddening.

In Figure 1 we show three low-dispersion (limiting resolution ~ 6 Å) SWP echelle photowrites obtained of R Aqr (or the compact H II region) (SWP 24811) and features A and B (SWP 24810). UV continuum is present throughout the wavelength range of all three spectra. Lyman-α geocorona illuminates the entire aperture at 1216 Å. Emission lines from R Aqr (or the compact H II region) in SWP 24811 include O I, C II, Si IV and O IV] (blended), N IV] (weak), C IV, O III], N III], Si II (weak), and Si III] and C III] (partially blended).

Limited observing time on 1982 May 7, 1983 May 25, and 1983 December 25 prevented us from obtaining spectra at all three positions, as was possible for 1985 January 2 (Fig. 1). Accordingly, *IUE* observations for 1982 May 7, 1983 May 25, and 1985 December 25 do not include spectra at the farthest slit position. Only on 1985 January 2 did observing time permit a third pointing, where R Aqr was placed ~ 2".5 beyond the edge of the slit (SWP 24823; Fig. 1) in order to completely isolate feature B and totally eliminate scattered light contributions from R Aqr. The *IUE* FES slit position

TABLE 1

IUE OBSERVING PROGRAM

Date	SWP Camera[a]	LWP/LWR Camera[a]	Target	Exposure (s)
1982 May 7.....	16916	...	Jet	14400
	16918	...	H II Region	1800
	...	LWP 13189	H II Region	1200
	...	LWP 13188	Jet	2400
1983 May 25.....	20068	...	Jet	14400
	20069	...	H II Region	2400
	...	LWP 16016	Jet	5400
	...	LWP 16013	H II Region	1200
1983 Dec 25.....	...	LWP 2490	Jet	7200
	21874	...	H II Region	2400
	21873	...	Jet	14400
1985 Jan 2	24810	...	Jet	18000
	24811	...	H II Region	3000
	...	LWP 5131	H II Region	2400
	24823	...	Jet	18000
1985 Jul 14.....	26412	...	Jet	10380
1985 Aug 8.....	26569	...	H II Region	2700

NOTE—SWP: 1200–2000 Å; LWR or LWP: 2000–3200 Å.
[a]In the 10″ × 20″ entrance aperture.

for SWP 24823 indicated that less than 1% visible light from R Aqr entered the slit. In SWP 24810, we estimate that 5% of the visual light attributed to R Aqr entered the aperture. Routinely monitoring the FES counts of R Aqr every 15 minutes provided means of verifying that spacecraft pointing errors were kept negligible during the 300 minute exposures on the jet. Note that striations perpendicular to the continuum in SWP 24823 (Fig. 1) comprise a high-dispersion "ghost" image from a previous target.

All absolute line fluxes shown in Table 2 (H II region) and Table 3 (jet) were obtained using the extended-source reduction method involving sampling 15 pixel widths along the axis of the spectrum in the extraction process. However, because most of the prominent emission lines are not spatially extended, we have reextracted these SWP spectra using the line-by-line files, and recalibrated the data using the point-source reduction process for 9 pixel point-source extraction. This was done in order to determine whether an excessive amount of background noise was introduced in the extended-source method. However, a comparison between absolute line intensities obtained with the point- and extended-source method shows agreement within 3% for spectra obtained at both the H II region and the jet.

IUE observations of the R Aqr system were obtained over the course of 970 days on the dates shown in Figures 2 and 3. Owing to spacecraft pointing constraints, and the nearly 1 yr intrinsic light period of the Mira variable ($P = 387$ days), scheduling of *IUE* observations coincided with either visual light minimum (November–December) or visual light maximum (April–May). The position axes defined by the lines joining radio feature A (p.a. 45°) and feature B (p.a. 29°) with R Aqr were nearly parallel to the spectral dispersion. Spacecraft pointing constraints prevented us from orienting the axis of dispersion perpendicular to the mean axis of jet features, which would have provided both wavelength and spatial information in a single echelle exposure of the extended structure. Accordingly, multiple exposures were required (slit roll ~ 325°) in order to isolate the jet features.

SWP 24810 contains contributions from both feature A and feature B. In addition to the emission lines which were detected in the H II region, N V λλ1238, 1242 and He II λ1640 lines are also present (Table 3). Si III] λ1892 in the jet is generally weak compared with the central H II region. The continuum appears diffuse and extended perpendicular to the dispersion. Furthermore, a number of emission lines are not cospatial with the continuum, i.e., they appear displaced relative to the continuum. This is most apparent for N V, C IV, and He II. In context with the 6 cm radio morphology, the displacement of these emission lines relative to the UV continuum suggests that they are more closely associated with radio feature A. On the other hand, the diffuse appearance of the UV continuum in SWP 24810 at wavelengths $\lambda \leq 1500$ suggests that the continuum is probably associated more with feature B, which is extended and resolved in the radio. We suspect that some of the lower excitation species such as O I, O III], and N III] are probably associated with feature B as well, because they are cospatial with the continuum.

The offset position of SWP 24823 completely isolated feature B, as well as feature A, from the H II region. The UV continuum appears weak and diffuse. Emission from C II, C III], and C IV, in addition to most (or all) of the lines detected in the central region, is present. Five weak and

TABLE 2

EMISSION LINES IN CENTRAL R AQUARII H II NEBULA

Ion	λ(lab)	1982 MAY 7		1983 MAY 25		1983 DEC 25		1985 JAN 2		1985 AUG 8	
		λ(*IUE*)[a]	Flux	λ(*IUE*)[a]	Flux	λ(*IUE*)[a]	Flux	λ(*IUE*)[a]	Flux	λ(*IUE*)[a]	Flux
N V[b]	1238.8, 1242.8	1240.2	Weak	...	...	1242.7	Weak	1245.8	1.0	1242.0	1.3
S II[c]	1250.5, 1253.8, 1259.5	1254.1	3.0	1252.2	Weak	?	...	1257.0	3.5	...	?
Si II[c]	1260.4, 1264.7, 1265.0	1265.8	Weak	1266.2	Weak	1262.2	2.0	1257.8	2.0	1261.9	Weak
O I	1304.9, 1306.0	1303.9	4.7	1308.0	7.9	1303.4	8.3	1301.9	7.0	1305.3	4.3
C II	1334.5, 1335.7	1335.8	6.2	1338.0	5.6	1332.7	1.8?	1331.1	5.0	1335.1	5.9
Si IV	1393.7	1393.2	1.0	1395.6	1.1	1392.7	0.4	1389.2	1.0	1393.9	1.5
O IV]	{1399.8, 1401.1 / 1404.8, 1407.4}	1402.9	5.0	1405.8	4.0	1400.3	3.4	1398.7	5.0	1402.5	6.4
N IV]	1486.5	1488.6	4.3	?	Weak	?	Weak	1480.6	1.8[d]	...	...
C IV	1548.2, 1550.8	1549.2	32.0	1553.1	29.0	1548.8	29.0	1546.7	30.0	1549.5	27.0
[Ne V][d]	1575.2	...	...	1576.4	Weak	1575.2	Weak	...	...	...	...
[Ne IV][d]	1601.5	...	...	1604.6	1.0	1605.2	Weak	...	...	...	...
He II	1640.5	...	...	...	1.2	1636.2	1.5	1635.6	0.8	1641.2	Weak
O III]	1660.8, 1661.1	1662.5	6.2	1668.8	7.0	1663.3	4.8	1660.7	9.5	1665.8	5.4
N IV?	1718.5	...	...	...	...	...	...	1721.8	1.7	1727.0	Weak
N III]	{1748.6, 1749.7 / 1752.2, 1754.0}	1749.2	12.0	1753.6	9.0	1751.1	4.8	1749.2	7.0	1751.1	4.7
Si II[f]?	1808.8, 1816.9	1813.6	4.7	1821.0	1.2	...	1.2	1816.2	1.9	...	...
								1833.9	0.9	...	...
Al III	1854.7	...	...	...	...	...	...	1850.1	1.9	...	...
O III[e]	1872.8, 1874.9	...	...	...	...	...	...	1875.1	Weak		
Si III]	1892.0	1890.8	9.6	1895.5	7.0	1981.2	4.7	1887.8	5.0	1892.3	6.2
C III]	1906.7, 1908.7	1908.6	≥ 70.0[h]	1911.8	≥ 70.0[h]	1906.9	≥ 50.0[h]	1905.3	≥ 50.0[h]	1908.8	≥ 50.0[h]
[O III] + C II]	{2320.9 / 2323.5, 2324.7 / 2325.4, 2326.9, 2328.1}	2328.4	24.0	2326.2	18.0	...	...	2334.5	19.0	...	...
[O II]	2470.3	2471.2	9.0	2470.0	13.0	...	...	2479.5	8.1	...	...
Fe II	2599.4–2631.3 multiplet (1)	...	...	{2606.0 / 2619.0}	10.0	...	...	...	...	...	...
Fe II	2739.5–2755.7 multiplets (62), (63)	2750.6	8.5	2747.6	6.0	...	...	2757.0	6.0	...	...
Mg II (*h* and *k*)	2795, 2802.7	2799.4	44.0	2796.6	47.0	...	...	2805.5	27.0	...	...
He I[i] + [Ar IV]	{2829.1 / 2853.6?}	2836.0	5.0	2833.2	6.0	...	...	2841.5	5.0	...	...
He I	2945.2	2945.0	3.0	...	...	...	...	...	...	...	...
O III	3132.9	3127.0	4.0	...	...	...	...	...	...	...	...

NOTE.—Wavelengths in angstroms. Flux units are 10^{-13} ergs cm^{-2} s^{-1}; not corrected for extinction; weak flux: $\leq 10^{-14}$ ergs cm^{-2} s^{-1}.

[a] Previous paper (Michalitsianos and Kafatos 1982) corrected λ(*IUE*) for Δλ +4.3 Å blueshift due to jet offset in *IUE* 10″ × 20″ aperture.

[b] Possibly N V, but generally weak.

[c] Si II transition is multiplet (4). May possibly be H_2 λλ1257.8, 1271.9?.

[d] Diffuse, broad feature centered at ~1488 Å and tentatively identified N IV] λ1486.5.

[e] Possibly Fe II multiplets (43), (44), (45). Cf. Michalitsianos and Kafatos 1982.

[f] Also unidentified in spectrum of RR Tel (Penston *et al.* 1983).

[g] Seen also in spectrum of RR Tel (Penston *et al.* 1983).

[h] Saturated.

[i] Very likely blended feature because He I λ2829.1 should be weaker than He I λ2945.2.

FIG. 1.— *IUE* SWP echelle spectra obtained on 1985 January 2 and 3. The position of the *IUE* 10″ × 20″ entrance aperture is shown on the VLA 6 cm radio map obtained by Kafatos, Hollis, and Michalitsianos (1983) on 1982 September 25. The major axis of the *IUE* entrance aperture is oriented at 325° p.a.

SWP 24811: A 50 minute exposure obtained on 1985 January 3. The *IUE* entrance slit was positioned slightly south and west of R Aqr, to avoid contributions from extended features A and B (jet/spike). The echelle spectrum shows the uniformly illuminated Lyman-α geocorona slit at 1216 Å. Prominent emission lines of O I, C II, Si IV and O IV] (blended), N IV], C IV, O III], N III], Si II (weak), Si III], and C III] are present (see Table 1). Ultraviolet continuum is evident throughout the SWP wavelength range.

SWP 24810: A 300 minute exposure obtained on 1985 January 2. *IUE* slit positioned over the peak intensity contour at feature B. The spatial separation of features A and B of ~3.″5 is near the limiting resolution of *IUE* (~3″). The width of the continuum appears more extended perpendicular to the dispersion. Emission lines N V λλ1238, 1242 (doublet not resolved in low spectral resolution), He II λ1640, and unidentified emission at 1871.8 Å are evident, in addition to the emission lines identified above. Si III] λ1892 is weak in feature A+B (SWP 24810) compared with the greater intensity of this feature in SWP 24811. The continuum appears diffuse if compared with SWP 24811, reflecting spatial inhomogeneities of the extended nebular region. Line emission from N V, C IV, and perhaps He II is not cospatial with the UV continuum. Line emission may come predominantly from feature A, while feature B is responsible for most of the diffuse continuum emission.

SWP 24823: A 300 minute exposure with slit positioned farther from R Aqr; the star was approximately 2.″5 from the slit edge. Diffuse and extended continuum emission is evident, in addition to C II, C IV, N III] (weak), and C III]. Weak striations perpendicular to the spectrum are from a previous overexposed high-dispersion ghost spectrum.

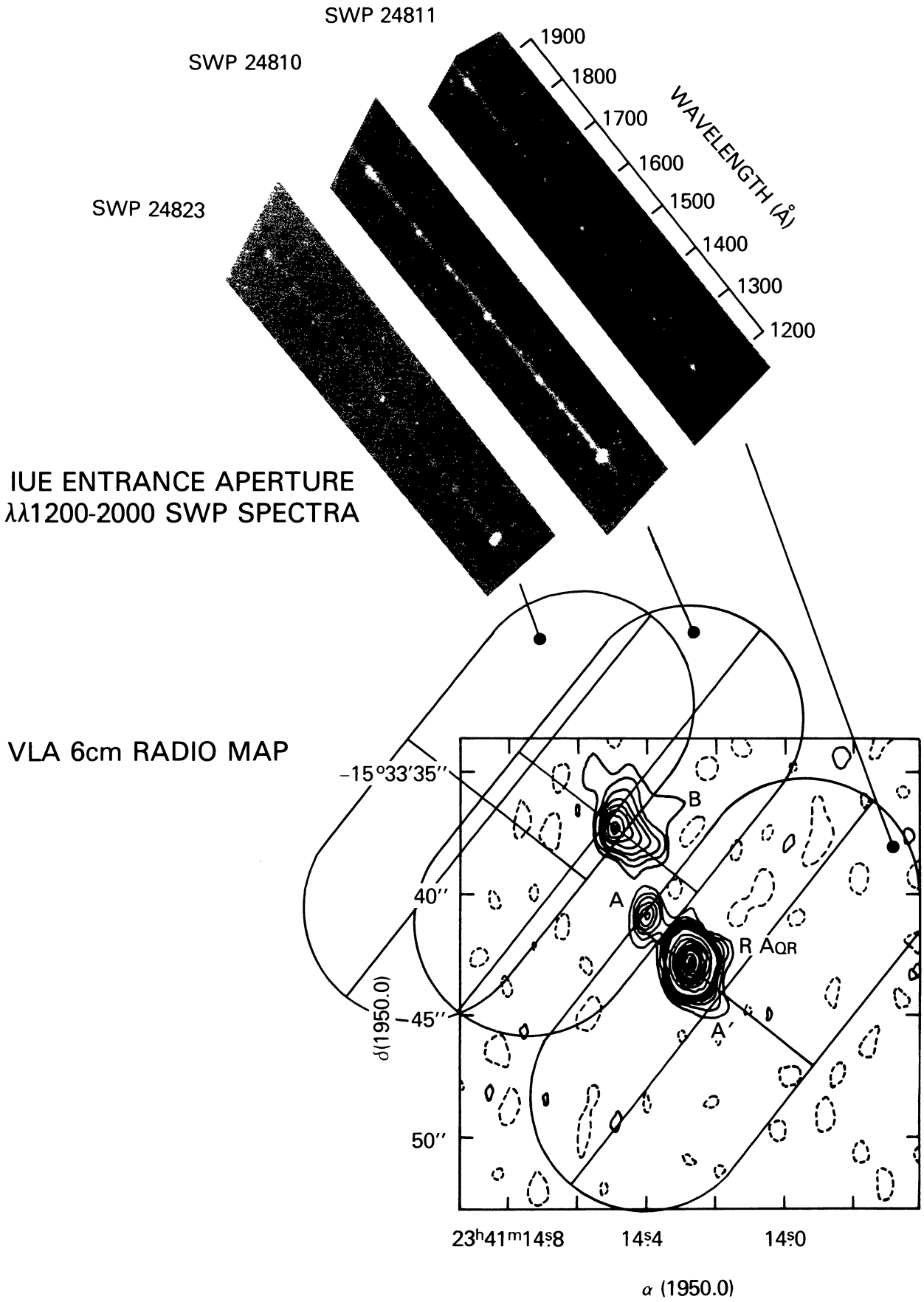

(This Page Intentionally Left Blank)

TABLE 3

EMISSION-LINE FEATURES A AND B (JET)

Ion	λ(lab)	1982 MAY 7		1983 MAY 25		1983 DEC 25		1985 JAN 2		1985 JUL 14	
		λ(*IUE*)[a]	Flux	λ(*IUE*)[a]	Flux	λ(*IUE*)[a]	Flux	λ(*IUE*)[a]	Flux	λ(*IUE*)[a]	Flux
N V	1238.8, 1242.8	1240.5	Weak	1238.5	0.8	1242.9	1.0	1240.2	4.2	1231.8	2.0
S II[b]	1250.5, 1253.8, 1259.5	1259.8	Weak	1260.2	Weak	1261.9	Weak	1260.7	Weak	1259.2	Weak
Si II[b]	1260.4, 1264.7, 1265.0										
O I	1304.9, 1306.0	1301.2	1.8	1303.4	3.9	1308.2	1.8	1305.6	1.5	1303.1	1.2
C II	1334.5, 1335.7	1331.4	0.9	1333.4	2.2	1338.0	2.4	1335.6	3.0	1327.8	3.0
Si IV	1393.7	1385.6	0.3	1391.1	0.3	1398.4	0.4	1393.2	0.8	1386.3	0.7
O IV]	1399.8, 1401.1	1397.4	0.5	1398.8	1.3	1406.2	0.8	1403.4	2.5	1394.7	0.7
	1404.8, 1407.4										
H_2?	1431.0	...	...	...	...	...	...	...	...	1430.0	2.0
N IV]	1486.5	1488.8	0.4	1485.8	1.6	1484.4	2.0	1486.1	1.1	1484.9	0.7
C IV	1548.2, 1550.8	1545.3	2.2	1546.6	7.0	1552.7	4.9	1550.2	≥15.0[c]	1542.2	9.5
[Ne V][d]	1575.2	1577.8	Weak	...	...	1574.0	Weak	...	...	...	...
[Ne IV][d]	1601.5	1605.1	Weak	...	...	1610.1	Weak	...	...	...	...
He II	1640.5	1634.8	0.7	1636.4	1.8	1646.1	0.3	1642.0	2.0	1634.8	1.1
O III]	1660.8, 1661.1	1661.4	1.5	1663.2	1.6	1666.5	1.1	1666.9	2.5	1659.2	1.0
N III]	1748.6, 1749.7	1746.7	0.7	1749.2	1.6	1752.5	1.5	1751.4	2.8	1747.8	3.2
	1752.2, 1754.0										
Si II	1808.0, 1816.9	...	...	...	...	1819.5	0.8	1818.8	0.3	...	...
O III[e]	1872.8, 1874.9	...	...	...	...	...	...	1871.8	0.4	1876.0	Weak
Si III]	1892.0	1887.6	≤ 0.1	1889.3	0.4	1894.1	0.4	1893.0	0.6	1889.5	0.5
C III]	1906.7, 1908.7	1903.4	~ 7.0	1904.6	≥13.0[c]	1909.8	≥14.0[c]	1909.5	≥ 9.0[c]	1903.0	≥13.0[c]
[O III] + C II]	2320.9, 2323.5, 2324.7, 2325.4, 2326.9, 2328.1	2333.0	5.4	2328.0	8.0	2321.5	6.9	...	...	...	...
[O II]	2470.3	2464.0	1.9	2473.4	3.0	2466.0	3.6	...	6.0	...	7.5
Mg II (*h* and *k*)	2795.5, 2802.7	2801.0	5.5	2798.4	9.0	2797.0	9.7	...	...	...	...
O III	3132.9	3129.0	1.5	...	...	...	...	...	...	...	...

NOTE.—Wavelengths are in angstroms. Flux units are 10^{-13} ergs cm^{-2} s^{-1}; not corrected for extinction; weak flux: $\leq 10^{14}$ ergs cm^{-2} s^{-1}.

[a] Michalitsianos and Kafatos 1982 corrected λ(*IUE*) for Δλ +4.3 Å blueshift due to jet offset in 10″ × 20″ *IUE* entrance aperture.

[b] Si II transition is multiplet (4). May possibly be H_2 λλ1257.8, 1271.9.

[c] Saturated.

[d] Possibly Fe II multiplets (43), (44), (45); cf. Michalitsianos and Kafatos 1982.

[e] Seen also in spectrum of RR Tel (Penston *et al.* 1983).

partially blended emission lines at 1254.7, 1261.4, 1265.8, 1280.0, and 1287.5 Å are seen in all SWP spectra obtained at the jet offset positions. Emission at 1261 and 1265 Å is possibly attributed to Si II multiplet 4 (λλ1260.4, 1264.7; see below). The remaining lines are possibly blends of Al III and C I, although definite identification is not possible. Although the signal-to-noise ratio achieved in SWP 24823 is not as good as that obtained in SWP 24810, emission from He II and N V is not evident, which further supports the suggestion that N V and He II arise in feature A. Thus, these lines are only seen at the intermediate slit position (SWP 24810).

The presence of N V and He II emission at the intermediate offset position indicates that this region (feature A) has the highest excitation in the system, compared with the central compact H II nebula, where these lines are not detected. Accordingly, we believe that soft X-rays in the 0.25–1 keV energy range detected in 1985 with *EXOSAT* (Baratta *et al.* 1985) are also emitted mainly from the material associated with jet features rather than from the compact H II region.

A further indication which generally suggests that higher UV excitation conditions prevail in the jet as compared with the central H II region is provided by Si II. In spectra obtained of the central compact H II region (SWP 24811), Si II λλ1808, 1816 emission is evident but weak. Generally these Si II lines provide a good indication that moderate excitation conditions exist, i.e., $T_e \sim 10{,}000$–$20{,}000$ K. Note that weak emission features at 1260.8, 1265.3, and 1532.7 Å in SWP 24810, which we tentatively attribute to Si II emission, may indicate that higher excitation conditions exist in feature A. This follows because still higher electron temperatures are required to populate the $3s^24s(^2S_{1/2})$ upper level of Si II λ1526.7 and the $3s^33d(^2D_{1/2})$ upper level of Si II λ1260.4, from the ground level $(3s^23p)^2P_1^o$, compared with the moderately high temperatures that are required to populate the $3s3p^2(^2D_{3/2})$ level of λ1808. Even though the oscillator strengths for Si II λλ1526 and 1260 lines are greater than Si II λ1808 by factors (Shull, Snow, and York 1981) of ~ 42 and ~ 174, respectively, the Si II λλ1808, 1816 lines are more commonly seen because they intensify at moderate excitation chromosphere conditions. For example, at $T_e \sim 50{,}000$ K, Si II λ1265 can be stronger than λ1817 (cf. Jordan 1969). Accordingly, the presence of the Si II λλ1260, 1264, 1533 emission in feature A is consistent with the higher excitation conditions, also indicated by N V, O V, and He II.

III. DATA ANALYSIS

a) Emission Measure

i) *The Ultraviolet Continuum*

We assume that the distance d to R Aqr is 300 pc, in rough agreement with Solf and Ulrich (1985), who give $d \sim 200$ pc. Our *IUE* observations indicate that the absolute continuum

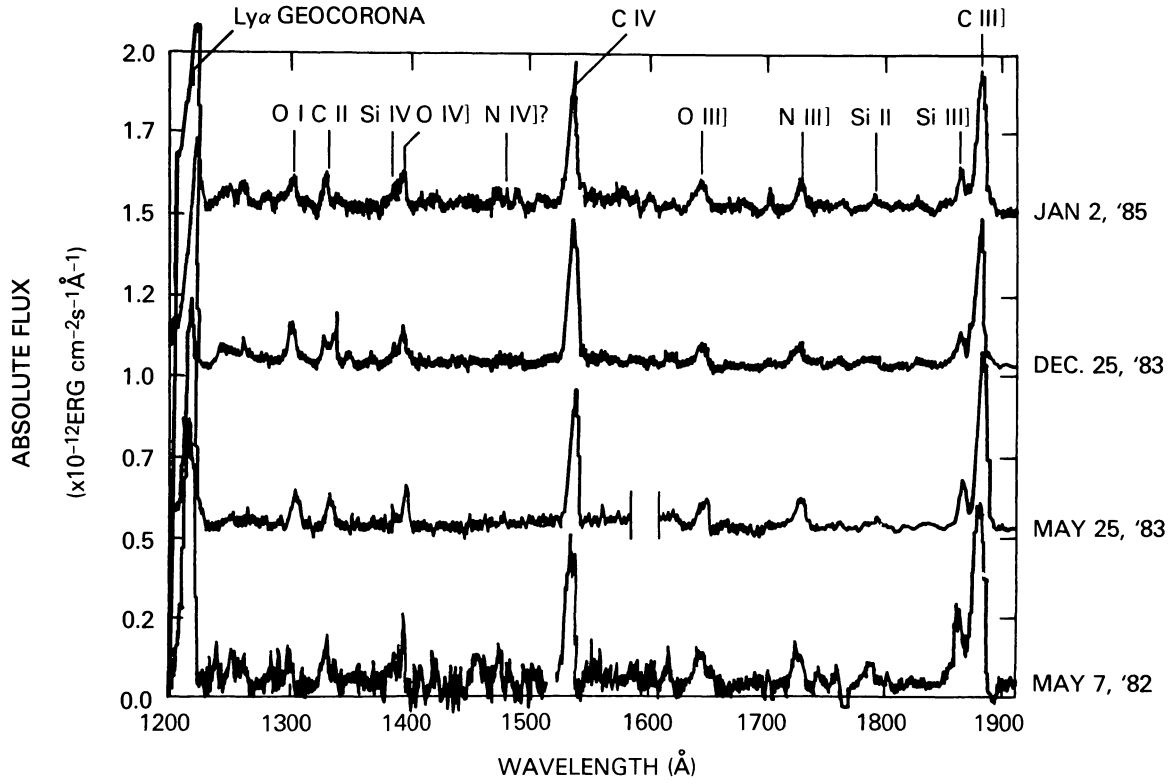

FIG. 2.—SWP 1200–2000 Å spectra of R Aqr (slit position as shown for SWP 24811 in Fig. 1) covering a time span of 970 days. Emission lines of O I, C II, Si IV and O IV] (blended), N IV] (weak), C IV, O III], N III], Si II, Si III], and C III] exhibit nearly constant absolute intensities. The continuum is flat, or independent of wavelength, and is not corrected for extinction. Each succeeding spectrum is incremented by 0.5×10^{-12} ergs cm^{-2} s^{-1} Å^{-1} on the absolute flux scale.

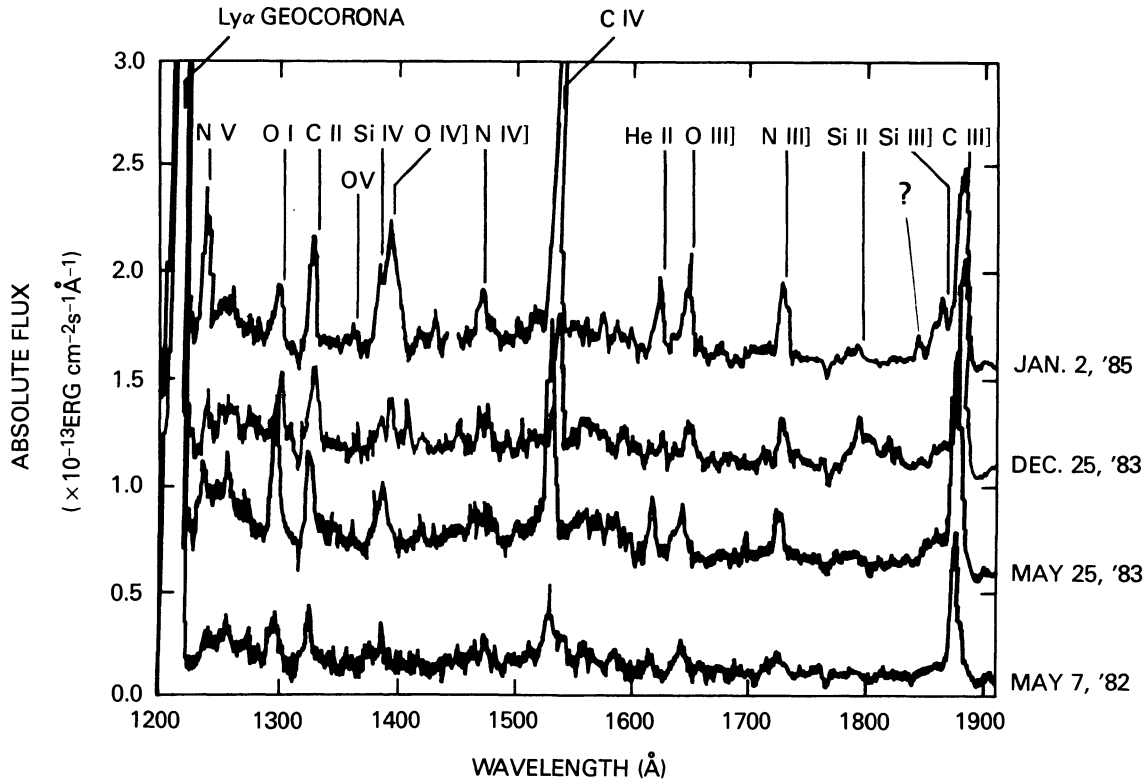

FIG. 3.—SWP 1200–2000 Å spectra of radio features B and A, with slit position as shown for SWP 24810 in Fig. 1. Note the different absolute flux scale compared with Fig. 2 (R Aqr). Each succeeding spectrum is incremented by 0.5×10^{-13} ergs cm^{-2} s^{-1} for comparison of different epochs. Note the presence of N V λλ1238, 1242 and He II λ1640, where N V appears variable over the time span of these observations. Si III] $3s3p\ ^3P^o \rightarrow 3s^2\ ^1S$ λ1892 is weak in the jet nebulosity compared with the central H II region.

flux from features A and B is $F_\lambda \sim (1-2)\times 10^{-14}$ ergs cm^{-2} s^{-1} Å^{-1} at $\lambda \sim 1500$ Å (see Fig. 3). We estimate that the two-photon continuum is dominant in feature B, while at 1500 Å feature A contributes at most 40% of the hydrogen two-photon continuum. Adopting an average electron temperature T_e for features A and B which we base on the C II ratio, $T_e \gtrsim 15{,}000$ K (see below), we find that about two-thirds of the total continuum detected is hydrogen two-photon emission, while about one-third is due to bound-free plus free-free continua if 40% of the continuum comes from feature A at 1500 Å. The emission measures for features A and B are given as follows: feature B, $n_e^2 L^3 \sim 1.8\times 10^{56}$ cm^{-3}, where L is the path length through the region (Kafatos, Michalitsianos, and Feibelman 1982); feature A: $n_e^2 L^3 \sim 2.7\times 10^{56}$ cm^{-3}. If, on the other hand, the continuum comes entirely from feature B, the emission measure of feature B is $n_e^2 L^3 \sim 3.9\times 10^{56}$ cm^{-3}.

For the central nebula, a lower limit to the emission measure is obtained if $E_{B-V} = 0$. It follows that if most of the UV continuum in spectra obtained of the central H II region (Fig. 2) comes from feature C1, then $n_e^2 L^3|_{C1}\xi \sim 1.6\times 10^{57}$ cm^{-3}, where the dimensionless factor ξ is $\gtrsim 1$ (see below), and $\xi \sim 1$ for a constant-density nebula. The value of the local reddening may be as high as $E_{B-V} = 0.65$ in the central nebula (Michalitsianos and Kafatos 1982), in which case $n_e^2 L^3|_{C1}\xi \sim 1.7\times 10^{60}$ cm^{-3}. This value represents an upper limit for the emission measure from the strongest radio feature C1.

ii) *The Radio Continuum*

1. *Jet features A and B.*—The emission measure can also be estimated from the VLA observations of Kafatos, Hollis, and Michalitsianos (1983) and Hollis *et al.* (1985). In the case of radio continuum emission, the UV continuum is not a sensitive function of T_e. We find that

$$n_e^2 L^3|_B \sim 2\times 10^{56}\ \text{cm}^{-3} \quad \text{(feature B)}$$

and

$$n_e^2 L^3|_A \sim 5.9\times 10^{55}\ \text{cm}^{-3} \quad \text{(feature A)}.$$

Combining the results from the two extreme cases of the UV and radio continuum, we adopt the following values of emission measures for features A and B:

$$n_e^2 L^2|_A \sim 1.1\times 10^{56}\ \text{cm}^{-3} \quad \text{(feature A)},$$

$$n_e^2 L^3|_B \sim 2.4\times 10^{56}\ \text{cm}^{-3} \quad \text{(feature B)}.$$

2. *Central* H II *nebula features C1 and C2.*—The radio observations (Hollis *et al.* 1986) indicate that the radio flux density of feature C1 is ~ 6 times stronger than C2 at $\lambda = 2$ cm, i.e., most of the UV continuum as well as the radio continuum originates from feature C1. The two features have approximately equal sizes, although C2 appears smaller, i.e., $L_2 \lesssim L_1 \sim 0''.4$ and are separated by $\sim 0''.5$. The strongest feature C1 is southwest of C2.

The question arises whether feature C1 arises from a wind, in which case the density would vary with distance away from the binary system. Applying the formalism of Wright and Barlow (1975), and applying the 2 cm radio data of Hollis *et al.* (1985) for a hot subdwarf wind, we find ($d = 300$ pc)

$$\dot{M} \sim 3\times 10^{-9} v_\infty\ M_\odot\ \text{yr}^{-1},$$

where v_∞ is the terminal wind velocity far from the star. For values of v_∞ ranging from the observed 200 km s^{-1} (Johnson 1981) to a hypothetical 800 km s^{-1}, which may be appropriate for the secondary star in R Aqr, as we have found for a similar system, RX Pup (Kafatos, Michalitsianos, and Fahey 1985), we obtain $6\times 10^{-7} \lesssim \dot{M} \lesssim 2.3\times 10^{-6}\ M_\odot$ yr^{-1}.

Similar values of $\dot{M} \sim 3.4\times 10^{-7}\ M_\odot$ yr^{-1} ($v_\infty \sim 50$ km s^{-1}) are obtained for the Seaquist, Taylor, and Button (1984) model. In this model (see also Hollis *et al.* 1985) the cool wind from the Mira variable is photoionized by the hot subdwarf.

Defining an average density in the wind as $n_e = \int n_e(r)\,dV/V$, where r is the distance from the star and V is the volume, and the limits of integration extend from an inner radius R_i to an outer radius of the photoionized wind R ($R = 0''.2$), we find

$$n_e = 3n_0(R - R_1)/\left(R^3 - R_i^3\right), \tag{1}$$

where $n_0 = \dot{M}/4\pi v \mu m_{\rm H}$ and μ is the mean molecular weight. Any continuum (or line) emission is proportional to the emission measure, $\text{EM} = \int n_e^2\,dV$, where

$$\text{EM} = n_0 4\pi(1/R_i - 1/R). \tag{2}$$

Defining an "average" emission measure $\text{EM} \equiv n_e^2 V$, we find

$$\text{EM} = \overline{\text{EM}}\,\xi,$$

where

$$\xi = \tfrac{1}{3}\left(R^3 - R_i^3\right)/\left[(R - R_i)R_i R\right]. \tag{3}$$

We can compare two extreme cases: (i) if $R \gg R_i$, then $\xi \to \frac{1}{3}R^2/R_i$; if, for example, R_i is the Mira radius 300 $R_\odot$ (Kafatos and Michalitsianos 1982), then $\xi \sim 10$; (ii) if $R_i \sim R$ (constant density), then $\xi \to 1$.

In what follows we use the mean values, because, in the extreme case, ξ corresponds to values only as large as 10. Typical values of density for C1 are

$$n_e \sim 10^6\left(\dot{M}/3\times 10^{-7} M_\odot\ \text{yr}^{-1}\right)\left(v/50\ \text{km s}^{-1}\right)^{-1} \times (R/0''.2)^{-2}\ \text{cm}^{-3}.$$

To reconcile the radio observations with the ultraviolet requires $\xi \gtrsim 1$, if $E_{B-V} = 0.65$ (otherwise n_e would be in excess of $\gtrsim 2\times 10^7$ cm^{-3}). More moderate values of $E_{B-V} \sim 0.2$ would yield, for C1, $n_e \sim 10^6$ cm^{-3} from the UV, in agreement with the radio estimate obtained above.

b) Electron Density

i) *The* C III *Line Ratio*

Values of n_e in the central nebula C1 obtained above are $n_e \sim 10^6$ cm^{-3}. Johnson (1981) argues for a value $\gtrsim 4\times 10^5$ cm^{-3} in the central nebula, owing to the absence of C III]

λ1906.7 emission. Two of us (M. K. and A. G. M.) carried out a collaborative HIRES SWP *IUE* program with a European team led by C. Jordan. We found that the ratio $I(\lambda 1906.7)/I(\lambda 1908.7) \sim 0.8$ applies to features A and B. Using the results of Nussbaumer and Schild (1979), and adopting an electron temperature $T_e \sim 20{,}000$ K appropriate for features A and B, we find $n_e \sim 3\times10^4$ cm^{-3}. This value probably applies primarily to feature A, because C III] line emission from feature B is weak.

ii) *The* Si III] *Line Ratio*

The ratio $I(\lambda 1882.7)/I(\lambda 1892.0)$ had the values (features A and B) 0.4 (1983 May 25), 1.16 (1983 December 25), 0.63 (1985 January 2), and 0.24 (1985 July 14). These results are consistent with a constant ratio $\sim 0.5^{+0.7}_{-0.25}$ because of the weakness of the Si III] lines in features A and B. Using the results of Nussbaumer (1986), we find a value of $\sim 5\times10^4$ cm^{-3}, in agreement with the value of $\sim 3\times10^4$ cm^{-3} obtained from the C III] ratio.

iii) *The* N IV] *Line Ratio*

The 1483,1487 Å feature is broad, indicating that the ratio is ~1:1, from which it follows that (Nussbaumer and Schild 1981) $10^4 \lesssim n_e \lesssim 10^5$ cm^{-3} applies for features A and B.

c) *Path Lengths and Column Densities*

Using the results of Hollis *et al.* (1985) and Hollis *et al.* (1986), and combining the results of previous §§ III*a* and III*b* above, we obtain

Feature C1:

$$L_{C1} \sim 1.8\times10^{15} \text{ cm},$$

$$n_e L|_{C1} \sim 1.8\times10^{21} \text{ cm}^{-2},$$

Feature C2:

$$L_{C2} \lesssim 1.8\times10^{15} \text{ cm},$$

$$n_e L|_{C2} \lesssim 7.3\times10^{20} \text{ cm}^{-2} \quad [\text{for } n_e|_{C2} \sim 4\times10^5 \text{ cm}^{-3}],$$

Feature A:

$$L_A \sim 5\times10^{15} \text{ cm} \quad (\sim 1''),$$

$$n_e L|_A \sim 1.5\times10^{20} \text{ cm}^{-2},$$

Feature B:

$$L_B \sim 1.3\times10^{16} \text{ cm} \quad (\sim 3''),$$

$$n_e L|_B \sim 1.3\times10^{20} \text{ cm}^{-2},$$

where L and $n_e L$ are the path length and column density, respectively.

We note immediately the constancy of column density in features A and B, i.e., $n_e L|_A \sim n_e L|_B$. It is even conceivable that $n_e L|_{C2} \sim n_e L|_B \sim n_e L|_A$, given the uncertainty in estimating the exact linear size of C2 from VLA observations. For the foregoing, the electron density n_e and linear dimension L of the jet features are empirically dependent on distance r from C1 as follows:

$$n_e^2 L^3 \propto r, \quad L \propto r, \quad n_e L \propto \text{constant}. \tag{4}$$

d) *Electron Temperature*

Electron temperatures in the central H II region (C1) and jet, which is a mean of both features A and B, can be obtained with the C II line ratios $I(\lambda 2325)/I(\lambda 1335)$ (Hayes and Nussbaumer 1984). These ratios for different epochs can be obtained from Tables 2 and 3. Unfortunately, because we do not have LWP coverage for all epochs, the 2325 Å intensity is unknown for some epochs, and must be interpolated. We find that the jet electron temperatures T_e are

1982 May 7: $T_e > 14{,}100$ K,

1983 May 25: $T_e > 16{,}800$ K,

1983 December 25: $T_e \sim 18{,}800$ K,

For the central H II region we have

1982 May 7: $T_e \sim 16{,}800$ K,

1983 May 25: $T_e \sim 18{,}800$ K,

1985 January 2: $T_e \sim 17{,}400$ K.

Our uncertainty in estimating T_e for both the central H II region and the jet is $\sim \pm 1500$ K. Thus T_e is the H II region appears constant over 4 years, with an average electron temperature $T_e \sim 18{,}000$ K. On the other hand, the electron temperature of the jet may be increasing over the period of these observations.

The optical line intensities (Wallerstein and Greenstein 1980) can be used to check the values obtained above for n_e and T_e. Even though the optical observations refer to an earlier epoch compared with these *IUE* observations, they nevertheless provide a check. For small values of $E_{B-V} \sim 0.0$–0.2 for the jet, we find that the [O III] line ratio $[I(\lambda 4959) + I(\lambda 5007)]/I(\lambda 4363)$ yields values of $T_e \sim 20{,}000$ K ($E_{B-V} \sim 0.2$). For the central H II region, Wallerstein and Greenstein (1980) find a larger extinction of $E_{B-V} = 0.65$. Thus, if $E_{B-V} \sim 0.65$ and $n_e \sim 3\times10^6$ cm^{-3}, the electron temperature of the central H II is $T_e \sim 15{,}000$ K.

A question naturally arises as to whether the electron temperature is different in features A and B. Because of limited observing time, it was possible only in 1985 January to obtain a third SWP spectrum of feature B at the extreme offset position. We find that emission from feature B is weak (SWP 24823; Fig. 1). We find that feature B can contribute at most 25% of the total emission from feature A and B combined in the lines of C III], C IV], and N III], and less than 10% in N V. Feature B could, however, contribute approximately 60% of the total emission from feature A and B combined in

C II, and as much as 100% in Si II. These relative contributions indicate generally a lower electron temperature for feature B compared with feature A.

Different electron temperatures in features A and B could in principle be obtained from knowledge of the relative contributions of the C II λλ1335 and 2325 intensities from features A and B. From the present data, we find that $10^4 \lesssim T_B \lesssim 16{,}000$ K, whereas $T_A \gtrsim 14{,}000$ K. We also find that the extinction in the jet features is small, i.e., $E_{B-V} \sim 0.2$. This value obtained from the C II ratios is consistent with the values of extinction derived from the ionic abundance analysis.

e) *Ionization Temperature*

i) *Fluorescent Lines*

Rough estimates of the ionization temperature, T_*, can be obtained from the strength of the line O III λ3133. The fluorescent lines of O III are, of course, connected with the photoionizing He II continuum ($h\nu > 54.3$ eV). For a value of $E_{B-V} = 0.2$, we find, assuming a blackbody photoionizing continuum, $T_* \sim 90{,}000$ K (this value again refers to some effective mean between features A and B). If E_{B-V} is as large as 0.4, then $T_* \sim 120{,}000$ K. The corresponding value of the central nebula is $T_* \sim 80{,}000$ K for $E_{B-V} = 0.65$.

ii) *X-Ray Emission*

Much higher temperatures of 5×10^5 K are obtained from the *EXOSAT* observations of 1985 (Baratta *et al.* 1985). The *EXOSAT* observations cover the range 0.2–1 keV, i.e., a softer energy range compared with *HEAO* B observations of Jura and Helfand (1984). This sensitivity difference may explain the marginal *HEAO* B detection obtained by Jura and Helfand (1984), if the X-ray–emitting region is $T_* \leq 500{,}000$ K (R. Viotti 1986, private communication).

f) *Ionic Abundances*

To obtain the ionic abundances we use the method of Michalitsianos, Kafatos, and Hobbs (1980) and Kafatos, Michalitsianos, and Hobbs (1980). For collisionally excited lines we have

$$N_{A,Z} \propto T_e^{1/2} \exp(\Delta E/kT_e)(n_e^2 L^3)^{-1} \times d^2 (n_A/n_{A\odot})^{-1} (10^{f_\lambda E_{B-V}}) \quad (5)$$

(cf. Osterbrock 1974), where $N_{A,Z}$ is the elemental ionic abundance A with charge Z, ΔE is the excitation energy, n_e is the electron density, L is the scale size, n_A is the elemental chemical abundance with atomic number A (relative to hydrogen), $n_{A\odot}$ is the solar chemical abundance of the same element (Cameron 1973), and $10^{f_\lambda E_{B-V}}$ is the extinction factor at the appropriate wavelength λ, tabulated by Seaton (1978).

Clearly, in order to compute $N_{A,Z}$, we need to know $n_A/n_{A\odot}$ and E_{B-V}. In the method of Michalitsianos, Kafatos, and Hobbs (1980) and Kafatos, Michalitsianos, and Hobbs (1980), use is made of the relation $\Sigma_{\text{all } Z} N_{A,Z} = 1$. However, only a few ionization stages are accessible in the *IUE* wavelength range, which makes abundance estimates with these assumptions difficult to determine. On the other hand, one can estimate whether any unobservable ions are present for a given epoch by analyzing emission lines of ions that are accessible in the *IUE* wavelength range. This is an iterative process. We can pick a reasonable value of E_{B-V}, hold n_A to its solar value $n_{A\odot}$, and maintain that the sum of all observable ionic abundances $N_{A,Z}$ is less than about 1. If convergence is not achieved, we select a new value of E_{B-V}, and repeat the calculation. Thus, iterations for elements that do not have solar abundances will diverge, requiring that we vary n_A, in order to achieve convergence. Additionally, we do not know the relative contributions of components A and B to the total absolute line flux directly from our *IUE* data. Thus, the values of $N_{A,Z}$ must be weighted for both components.

g) *Excitation and Elemental Abundance*

With the procedure described above, we find that the extinction in the jet is fairly small, $E_{B-V} = 0.2$. Also, the values of n_A are close to their solar values, except for silicon, which is underabundant by a factor of ~ 10 compared with the solar values. This underabundance has been seen before in other symbiotics, e.g., RW Hydrae (Kafatos, Michalitsianos, and Hobbs 1980), and RX Puppis for both silicon and carbon (Kafatos, Michalitsianos, and Feibelman 1982). In R Aqr, however, carbon seems to be normal. The depletion of silicon could be due to the presence of silicate grains that Johnson (1982) has deduced for the R Aqr nebula. The presence of SiO maser emission in R Aqr (Michalitsianos, Hollis, and Kafatos 1986) indicates that a fraction of silicon is in molecular form.

IV. DISCUSSION

Temporal variations of the absolute intensities of N V, C IV, and He II are shown, together with the visual 387 day light curve of the Mira variable, in Figure 4. The emission-line fluxes appear variable. Of the numerous UV lines observed from the combined emission of jet features A and B, N V, C IV, and He II exhibit the greatest amplitude variations, with C IV showing a factor of ~ 2 and He II showing a factor of ~ 6 variability, on a time scale of ~ 1.5 yr. As a very conservative estimate, we take error bars on the absolute line intensities of 15% (cf. Sonnenborn 1984) for well-exposed emission lines. The intensities of the C IV doublet were generally $\gtrsim 160$ DN, with 30–40 DN as the typical background noise level for 300 minute integrations. The signal-to-noise ratio in the *IUE* SWP camera for these emission lines at a given epoch is typically ~ 4–5.

In Figure 5 we show the absolute intensities for the strongest emission lines observed in the central H II region (*upper panel*), and the combined emission intensities (*lower panel*) of features A and B (the jet components). A trend of steadily increasing flux over 4 years of the combined emission of features A and B is evident, particularly in the high-excitation lines of C IV, He II, and N V (Fig. 4, *lower panel*). A similar trend is also evident for other, lower excitation emission lines, although not quite so pronounced, e.g., Mg II and C II. This effect is not observed in the central H II region (Fig. 5, *upper*

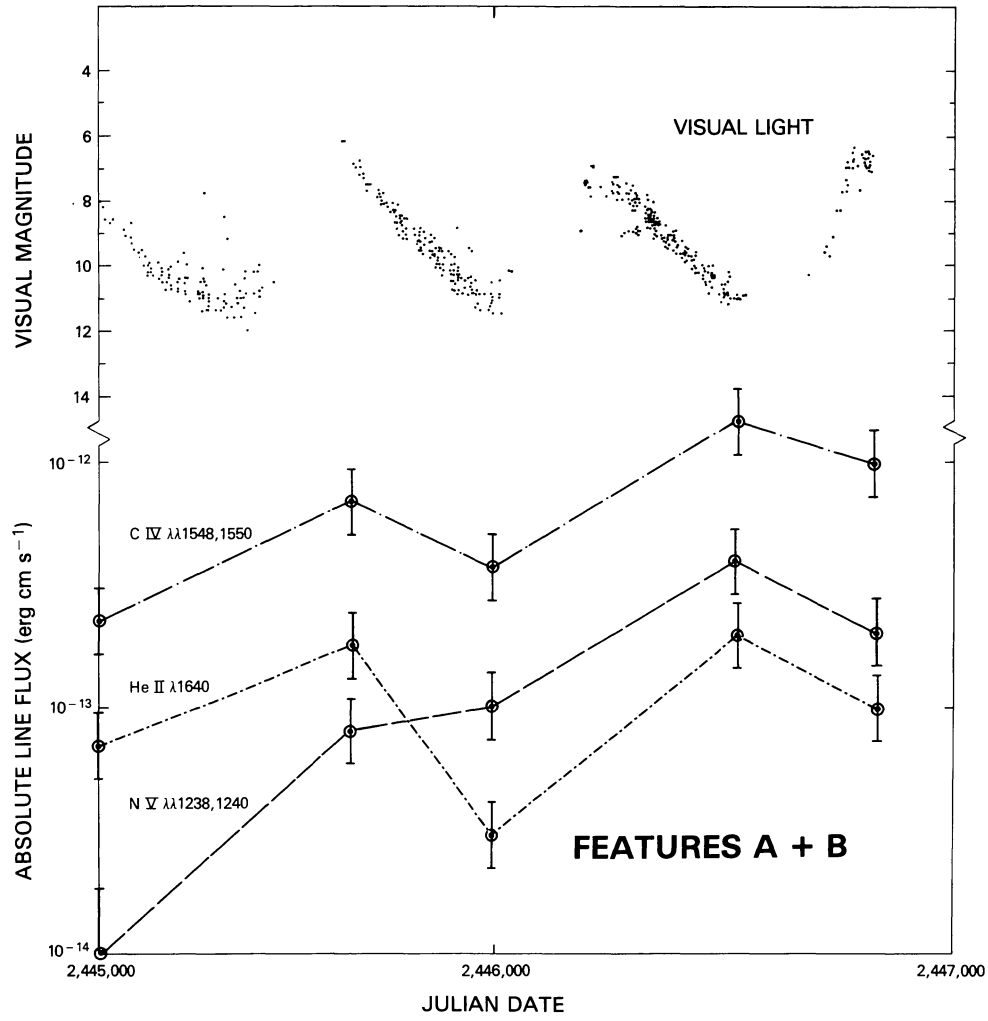

FIG. 4.—Temporal variations of the N V, C IV, and He II line intensities from the jet components A and B. The visual light curve of the Mira variable in R Aqr is also shown (AAVSO data, kindly provided by J. Mattei).

panel). Overall, the absolute intensities of combined emission from features A and B in N V, C IV, and He II appear to have increased by a factor $\gtrsim 4$ over 4 yr. The long-term variations in absolute sensitivity of the SWP camera estimated by Sonnenborn (1984) of roughly 10% is small compared with this systematic trend. Thus this trend appears real. We note that possible weak variations of the O III] and N III] lines in the central H II region are observed. The C II λ1335 line exhibited a large change on 25 December 1983, but this may be due to a radiation hit in adjacent pixels, producing an erroneous intensity estimate (Fig. 5, *upper panel*).

The absolute line fluxes obtained for the jet (features A and B) enable us to determine the electron temperatures for this region from § III*d*, and to determine the appropriate emission measures from § III*a*. Using equation (5), we compute the ionic abundances $N_{A,Z}$. These are shown in Figures 6*a* and 6*b*, where we have assumed $E_{B-V} = 0.2$. The ratios of ionic abundances are shown in Figure 7. Note, that, for the case of silicon, our observations confirm a depletion relative to solar abundance (i.e., the Si ionic abundances should be multiplied by a factor ~ 10). We have not shown the ionic abundances for the central H II region because T_e could be constant, and the line fluxes are not varying significantly, i.e., we suspect that $N_{A,Z}$ is fairly constant for the central H II region (components C1 and C2).

In Table 4 we show the relevant time scales for a cosmic gas of $n_e = 3 \times 10^4$ cm^{-3} (see § III*b*) and $T_e = 19{,}000$ K (see § III*d*), appropriate for feature A. The recombination time scale and collisional ionization time scale are, respectively,

$$t_R^{A,Z} \equiv 1/\alpha(A,Z)\, n_e$$

and (6)

$$t_I^{A,Z} \equiv 1/C(A,Z)\, n_e,$$

where $\alpha(A,Z)$, $C(A,Z)$ are the recombination and colli-

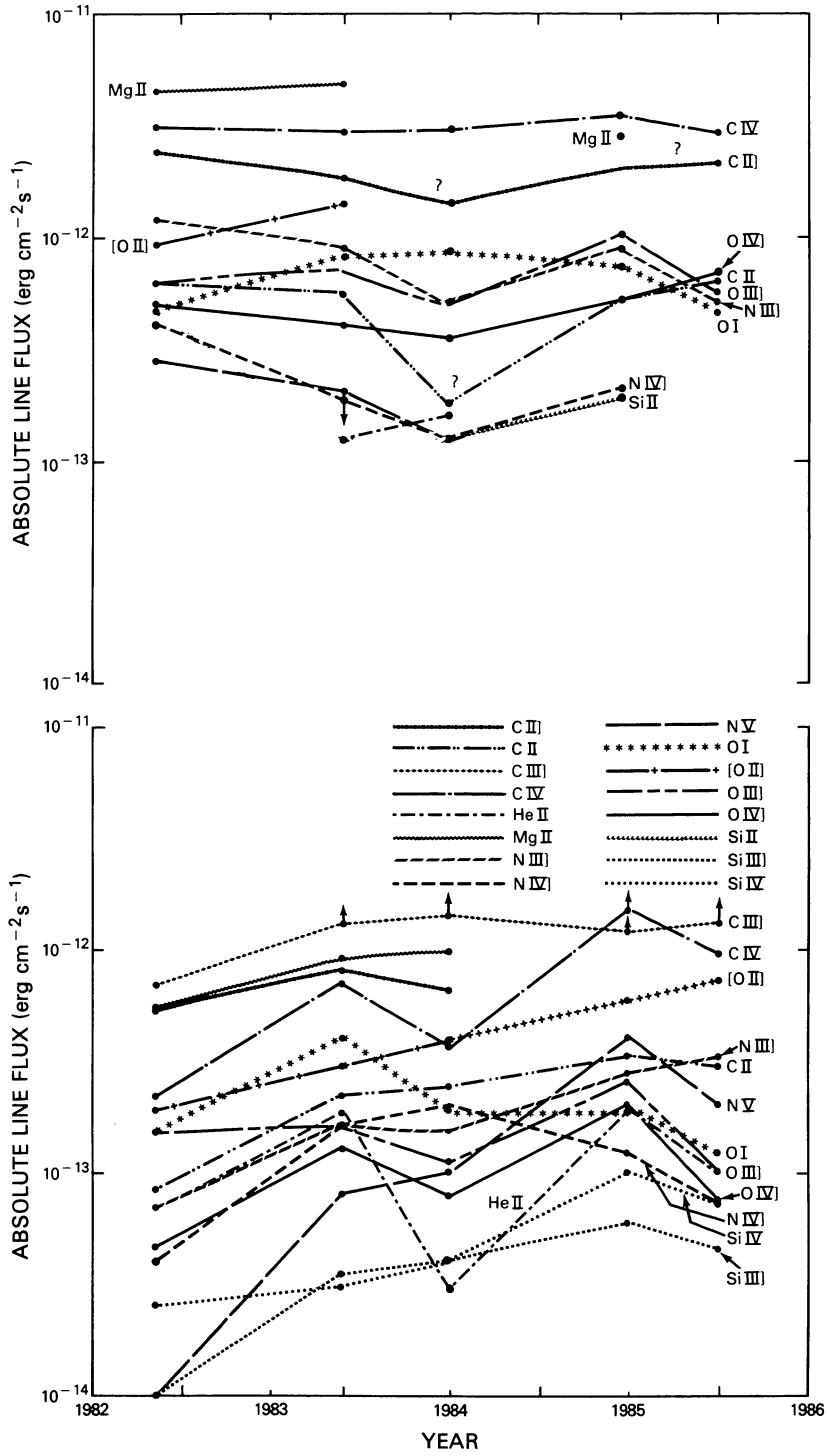

FIG. 5.—Absolute line intensities obtained from features A and B (*lower panel*) and from the central H II region (*upper panel*). An error of 15% is estimated for the absolute line-emission intensities.

sional ionization coefficients of an element with atomic number A and charge Z (Kafatos 1973).

The collisional ionization time scales are all very large except for neutral atoms. The recombination coefficients, however, are all short, ranging from ~ 0.1 to 6 yr (they would be 3 times as large for $n_e = 10^4$ cm^{-3}, which would be more appropriate for feature B). These recombination time scales are comparable to the time scale of the line fluxes (Figs. 4 and 5) and the ionic abundances (Fig. 6) to return to their minimum values after achieving their maxima (approximately

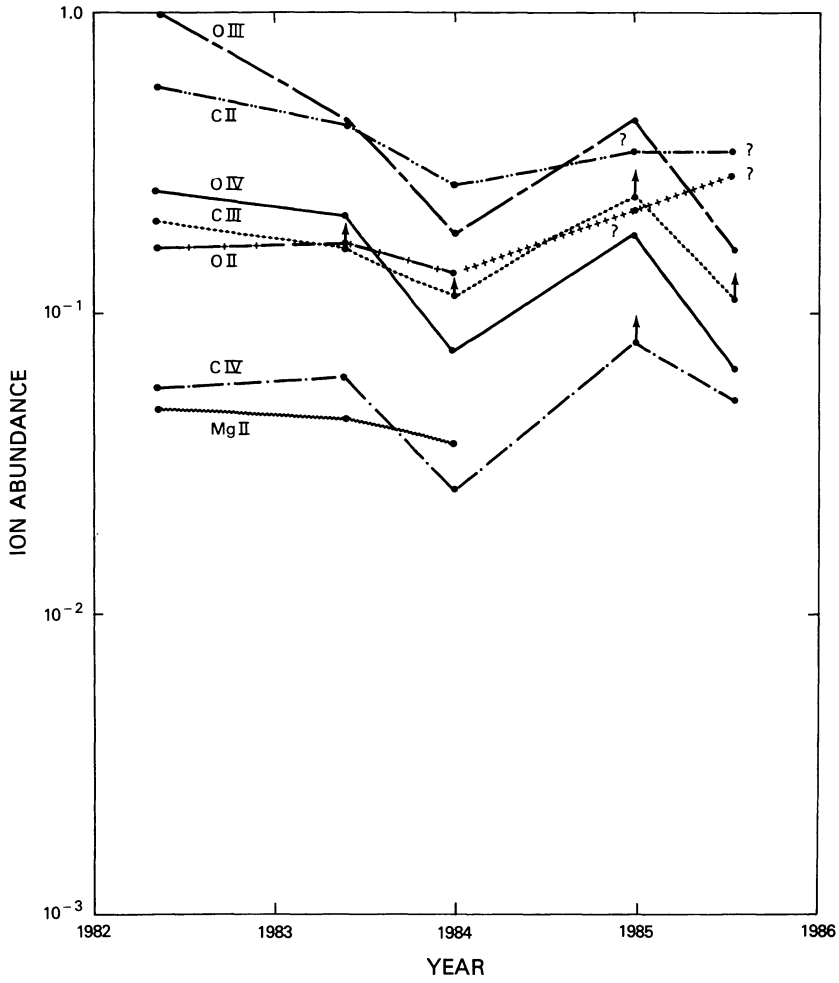

FIG. 6*a*

FIG. 6.—(*a*) Ionic abundances of the C, O, and Mg ions seen in the jet features A and B. (*b*) Same as in (*a*), but for the N and Si ions. The Si ionic abundances should be multiplied by the factor 10, because Si is underabundant by that factor.

0.5–1 yr). We conclude that collisional ionization, such as might occur in shock heating of features A and B, cannot explain the rise time indicated in Figures 4–6, but recombination could explain the fall time seen in the same figures.

The heating rate of the gas in featurere A can also be estimated as follows: the cooling rate $\Lambda \sim 4 \times 10^{-23}$ ergs cm^3 s^{-1} (Kafatos 1973), and the corresponding cooling time scale t_C for a gas at $T_e \sim 19{,}000$ K and density $n_e \sim 3 \times 10^4$ cm^{-3} is

$$t_C \equiv T(dT/dt)^{-1} = 3kT/(n_e \Lambda), \qquad (7)$$

where $t_C \sim 0.22$ yr. The rise time for T_e of features A and B is ~ 8 yr, which corresponds to a heating rate $H \gtrsim \Lambda$, and $H \sim 4.1 \times 10^{-23}$. We find (Osterbrock 1974; Spitzer 1978) that $H \sim (3/2)kT_* \alpha n_e^2$, where α refers to the recombination coefficient and T_* is the temperature characterizing the ionizing radiation. We estimate that T_* should be $\sim 8 \times 10^5$ K, which is comparable to the value deduced from the soft X-ray observations. We conclude that soft X-rays could be responsible for the heating seen in components A and B.

We can compute the ionization degree of hydrogen, x ($x = n_{\rm H}^+ / n_{\rm H}$), from the equation of ionization balance, which is

$$\frac{dx}{dt} = -\alpha n_{\rm H} x^2 + C n_{\rm H} x(1-x), \qquad (8)$$

where α and C are the recombination and ionization coefficients for hydrogen. Equation (8) is valid in the absence of a strong photoionizing continuum. We find that the solution of equation (8) after a time $t \sim 1.5$ y r, for $n_{\rm H} \sim 3 \times 10^4$ cm^{-3} (appropriate for the jet components) is $x_f \sim 0.9$. This result is fairly insensitive to the assumed initial ionized fraction x_i. A strong photoionizing continuum would increase x above the value of 0.9. We conclude that collisions alone can keep hydrogen mostly ionized, and that the gas in features A and B is primarily ionized hydrogen.

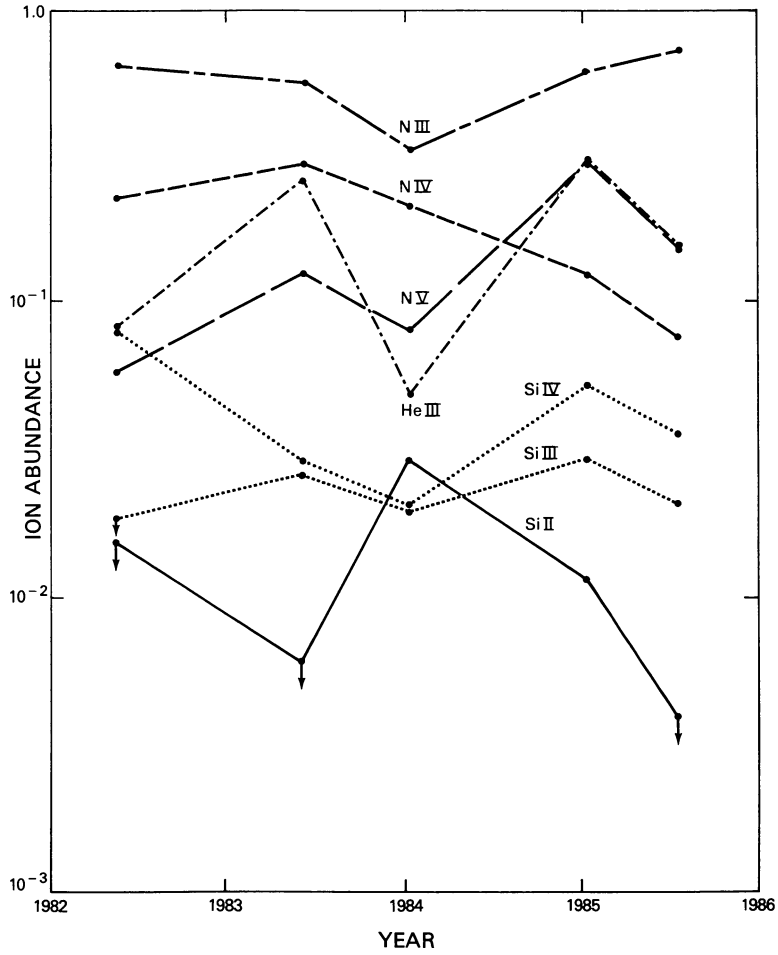

FIG. 6*b*

The rise time of the emission-line fluxes and the ionic abundances can be explained if the photoionizing continuum source is intrinsically variable on time scales of ~ 1.5 yr. On the other hand, if shocks are formed during phases of enhanced mass accretion, and transfer energy to the jet components, characteristic velocities must be ~ 6000 km s^{-1} in order to explain the ~ 1.5 yr variations observed in UV line fluxes, at the distances separating C1 from features A and B. Moreover, it is not clear how a shock could accelerate, ionize features A and B, and then decelerate, in order to account for the kinematics of the system (cf. Solf and Ulrich 1985).

The binary system is believed to consist of a 387 day period Mira variable ($m_V = 6.5$–11.0), and a hot $T_{\rm eff} \sim 25{,}000$ K subdwarf (Michalitsianos, Kafatos, and Hobbs 1980). The H II region (primarily component C1) accounts for the rich nebular emission-line spectrum that characterizes the optical and UV spectra of R Aqr. Originally, we suspected the jet was formed during eposides of mass transfer, one of which took place in the 1970s, when the Mira variable and the compact hot secondary were assumed near periastron (Kafatos and Michalitsianos 1982). It was assumed that mass transferred at super-Eddington rates results in the formation of a thick accretion disk, which produces a jet of collimated material, consisting of shocked parcels of gas which move at characteristic velocities ~ 1000 km s^{-1}, if they were expelled in the mid-1970s. Velocities of ~ 1000 km s^{-1} have subsequently been shown not to exist (Solf and Ulrich 1985).

An alternative model was proposed by Solf and Ulrich (1985). The origin of the inner north-south nebula and outer east-west nebula have been interpreted from high-resolution echelle spectra as the result of two distinct ejection events, separated in time by 450 yr, the most recent of which took place 180 yr ago. In this model, feature B ("spike") consists of material which was expelled 180 yr ago, but became visible in the mid-1970s, when it decelerated as a result of local drag of the flow in previously expelled material. This, according to Solf and Ulrich (1985), accounts for the appearance of feature B in the mid-1970s, its distance from R Aqr of $\sim 10^{16}$ cm, and the moderate heliocentric radial velocities of -60 km s^{-1} observed.

We note, however, that the cooling time for a few times 10^5 K ultraviolet- and soft X-ray–heated gas is ~ 1 yr (for $n_e \gtrsim 10^4$ cm^{-3}), which is small compared with the observed lifetime of feature B (probably a factor of 5–10 longer). From our most recent *IUE* observations, the ionization temperature of features A and B is steadily increasing, i.e., N V and He II

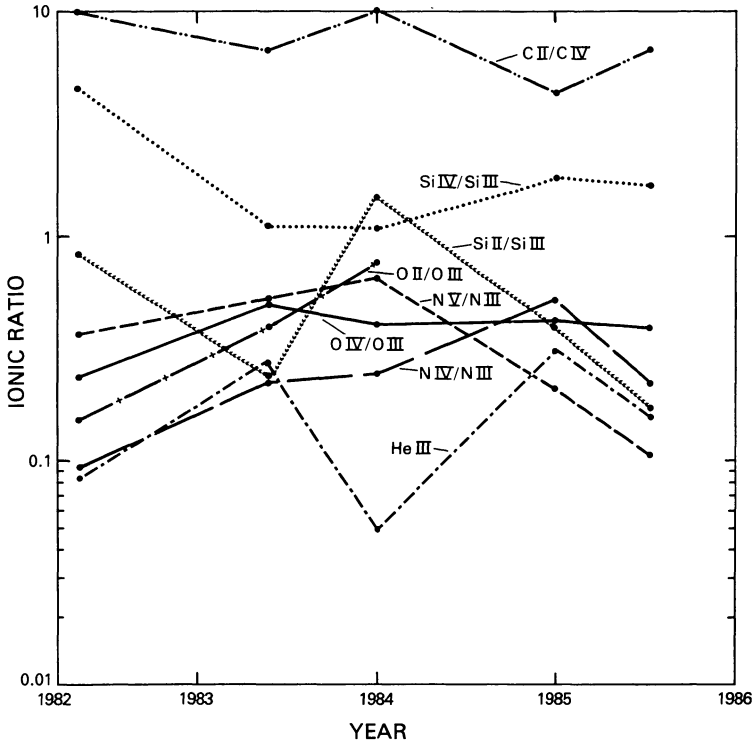

FIG. 7.—Ionic ratios for various ions seen in features A and B (see also Figs. 6*a* and 6*b*). The He III ionic abundance, rather than a ratio, is shown.

TABLE 4

TIME SCALES FOR A COSMIC GAS

Ion	Recombination Coefficient $\alpha(A, Z)$ ($cm^3\ s^{-1}$)	Collisional Ionization Coefficient $C(A, Z)$ ($cm^{-3}\ s^{-1}$)	Recombination Time Scale[a] $t_R^{A,Z}$ (yr)	Collisional Ionization Time Scale[a] $t_I^{A,Z}$ (yr)
H I.....	...	2.2×10^{-12}	...	0.48
H II	2.57×10^{-13}	...	4.11	...
C I.....	...	2.69×10^{-11}	...	0.04
C II	2.56×10^{-13}	9.56×10^{-6}	4.14	1.1×10^{3}
C III ...	1.86×10^{-12}	2.94×10^{-22}	0.57	3.59×10^{9}
C IV	3.03×10^{-12}	...	0.35	...
C V	6.19×10^{-12}	...	0.17	...
N I.....	...	3.29×10^{-12}	0.32	...
N II	2.07×10^{-13}	5.4×10^{-17}	5.10	1.95×10^{4}
N III ...	1.43×10^{-12}	...	0.74	...
N IV ...	3.44×10^{-12}	...	0.31	...
N V	7.11×10^{-12}	...	0.15	...
N VI ...	1.19×10^{-11}	...	0.09	...
O I.....	...	8.72×10^{-12}	...	0.12
O II	1.61×10^{-13}	2.0×10^{-18}	6.55	5.30×10^{5}
O III ...	1.27×10^{-12}	...	0.83	...
O IV	3.42×10^{-12}	...	0.31	...
O V	6.51×10^{-12}	...	0.16	...
Si I.....	...	3.42×10^{-10}	...	3.1×10^{-3}
Si II	2.57×10^{-13}	2.87×10^{-13}	4.11	3.68
Si III ...	1.39×10^{-12}	4.0×10^{-18}	0.76	2.65×10^{5}
Si IV ...	3.64×10^{-12}	...	0.29	...
Si V	7.11×10^{-12}	...	0.15	...

[a] Cooling time scale: $t_C \sim 0.22$ yr. These time scales correspond to $n_e = 3\times10^4\ cm^{-3}$ and $T_e = 19{,}000$ K (appropriate for jet component A); for other densities one should multiply the values given above by $(n_e/3\times10^4\ cm^{-3})^{-1}$.

emission detected in 1985 suggested that the rise time for T_e of the jet components (~ 8 yr) is long compared with the observed variability of the UV line intensities (~ 1.5 yr). We are not aware of any shock deceleration model that can produce quasi-periodic excitation conditions, while at the same time providing a slowly increasing electron temperature.

Finally, the distance of each jet parcel (C2, A, and B) from C1 is linearly dependent on position angle (Hollis *et al.* 1986). This suggests that the position of the jet components is highly dependent on the geometry of the system and the mode of expulsion (Hollis *et al.* 1986). Furthermore, it indicates that the formation of the jet components is probably not the result of chance encounters of differentially moving gas parcels in the inner north-south nebula (Solf and Ulrich 1985).

We have revised our previous model in order to explain the origin of the jet features by including the latest optical, UV, and radio data. We propose that parcels of material expelled during outbursts are photoionized by a cone of intense UV and soft X-ray radiation, which is formed by the inner edge of a thick accretion disk. As in our original model (Kafatos and Michalitsianos 1982), the disk becomes hot when material is transferred rapidly from the Mira variable to the hot subdwarf when the Mira fills its Roche lobe near, or at, periastron. A geometrically thick accretion disk formed during this transfer phase generates sufficiently high temperatures at its inner edge that most of the flux from the boundary layer/inner region is in the far-UV and soft X-ray energy range. The high column densities in the plane of the disk prevent X-rays from escaping in this direction. Thus X-rays would be more difficult to detect from the central H II region, if the disk is viewed nearly edge-on. This orientation is consistent with long-term variations of the visual light cycle of the 387 day Mira, which indicate that light from the Mira is partially obscured every 44 yr (Willson, Garnavich, and Mattei 1981).

If components C2, A, and B were formed during successive outbursts of the system, feature C2 would represent the most recent ejection, which took place in the mid-1970s. A comparison between the radio flux reported by Johnson (1980) at 85 GHz and by Hollis *et al.* (1985) at 1.5, 4.86, and 14.9 GHz (extrapolating the observed radio continuum to higher frequencies) suggests variability in radio emission. This indicates that the outbursts which formed the jet took place after Johnson's observations. The intensified radiation field of the disk during this most recent periastron passage also caused ejecta from previous outbursts, namely, components A and B, to brighten (Fig. 8).

The moderate radial velocities of $v_R \sim -60$ km s^{-1} observed in components A and B (Solf and Ulrich 1985) suggest that mass expulsion probably occurs at the outer edge of the disk, where the escape velocities are relatively small, i.e., $\lesssim 100$ km s^{-1}. Adopting a constant radial velocity for features A, B, and C2 of ~ 60 km s^{-1}, and using the distances which features C2, A, and B have with respect to C1, which, respectively, are 0".5, 2".7, and 6".4, we deduce that the individual jet components were expelled in the following order: feature B, 150 yr ago; feature A, 65 yr ago; and feature C2, 12 yr ago.

The ejection of feature A would have taken place in the early 1920s, i.e., about the time that P. Merrill recorded a spectroscopic outburst in the system. Component C2 would then correspond to the most recent ejection event, which took place between 1970 and 1975, which also coincided with a brightening of component B (Wallerstein and Greenstein 1980). Finally, the ejection of feature B took place ~ 3 orbital periods ago, if 1 orbital period of the binary is the time separating the ejection of features A and C2. Accordingly, $65 - 12 = 53$ yr is very roughly in agreement with independent estimates of the binary orbit period of ~ 44 yr (Willson, Garnavich, and Mattei 1981; Kafatos and Michalitsianos 1982; Wallerstein 1986). Our conclusions are opposed to the model of Solf and Ulrich (1985), who propose a single ejection event forming the inner nebula ~ 180 yr ago. Solf and Ulrich's observations, however, cannot provide any information on the structure of the jet at the sub-arcsecond level.

The simplest explanation for the ~ 1.5 yr variability observed in UV emission lines of components A and B probably involves variations of the ionizing flux of UV and X-ray photons originating in the boundary layer/inner disk. The time scale of ~ 1.5 yr may reflect a coupling of the Mira 387 day pulsation and mass transfer to the companion. This particular point is open to further investigation.

If radio components C2, A, and B are all illuminated by the cone of ionizing radiation, the cone must have an opening angle of 150° (Fig. 8). This follows because the radiative cooling time for C2, A, and B is $\lesssim 1$ yr. Accordingly, all three components must be continuously illuminated by the cone in order to explain their sustained radio flux over a few years and the recently enhanced level of N V and He II emission that we have detected in the combined emission from components A and B. This radiation field geometry is consistent with a thick accretion disk in the outer regions ($r \sim 10^{13}$ cm) (Fig. 8). We find that the inner region of the disk is thin (cf. Kafatos, Michalitsianos, and Fahey 1985), so that $h/r \sim 0.01$, where h is the disk half-thickness; this implies that the inner radius of the disk r_i (cf. eq. [5] of Kafatos, Michalitsianos, and Fahey 1985) is

$$r_i \sim (M_2/M_\odot)(T_d/5\times 10^5\ \mathrm{K})^{-1} \times 10^9\ \mathrm{cm}, \qquad (9)$$

where M_2 is the mass of the secondary and T_d is the temperature of the inner regions in units of 10^5 K, i.e., the temperature deduced from the soft X-ray observations, and from the previous discussion ($T_d = T_*$). A boundary layer of radius $\sim r_i$ would be several times hotter than the inner disk ($T_{\rm bl}/T_d \sim 5.8$).

The disk would be considerably extended in the outer regions, where it is also quite cool. The disk could be the source of obscuration of the Mira, reported in the late 1970s from *JHKL* photometry, that suggests temperatures in the outer regions $T_d \sim 1800$ K (Whitelock *et al.* 1983).

The low opacity normal to the disk plane allows X-rays to escape in the broad polar radiation cones. A fraction of the incident X-ray flux intercepted by the various components C2, A, and B is absorbed and thermalized, and produces high-excitation UV line and free-free emission. Thus, the components scatter a small fraction of the incident X-rays toward the observer. Adopting a distance of 300 pc, we determine an observed soft X-ray luminosity of $\sim 10^{31}$ ergs s^{-1} for R Aqr, in the 0.25–1 keV range, for a count rate

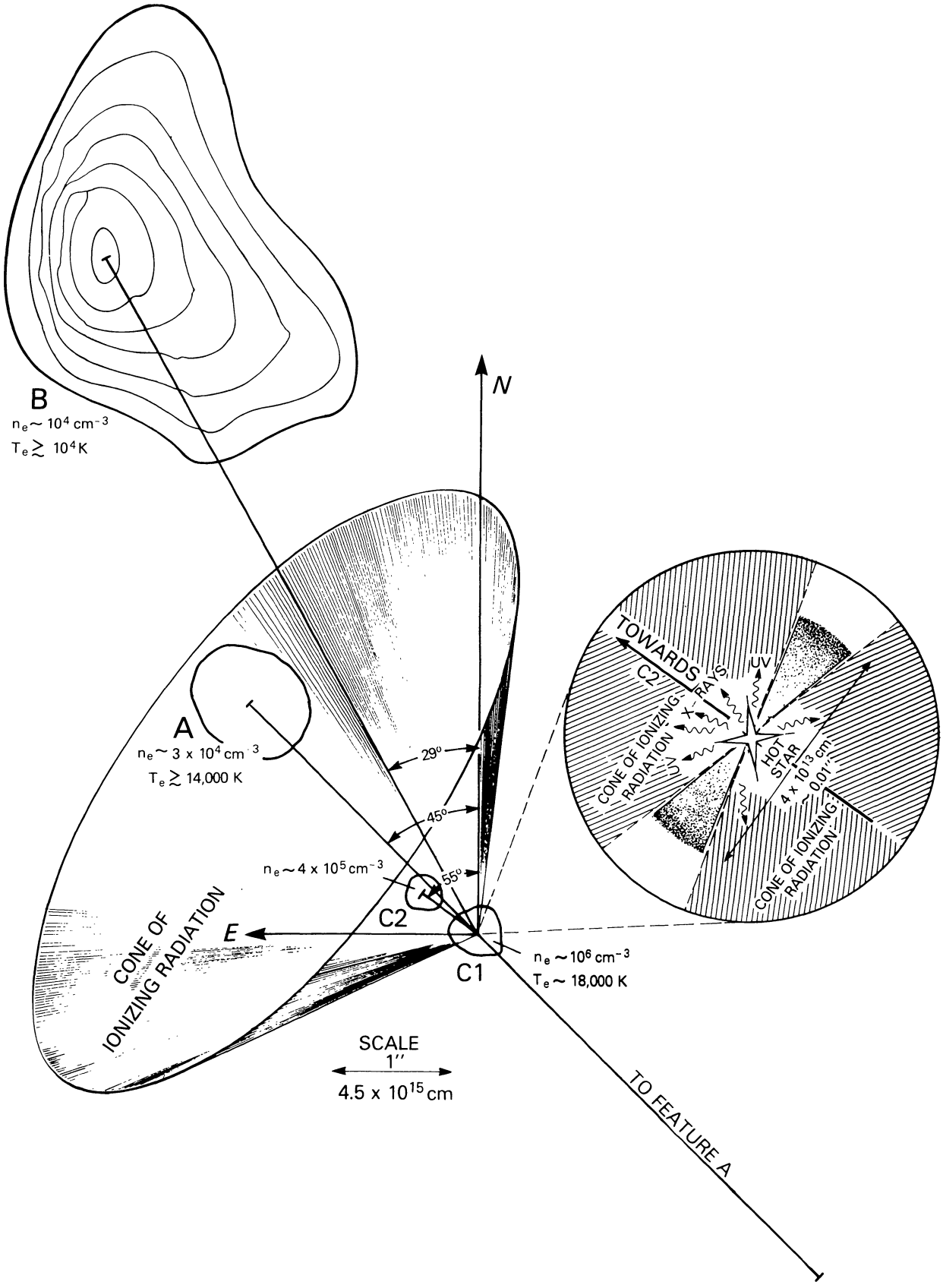

FIG. 8.—Our proposed model for R Aqr. The ionization is provided by a hot, inner accretion and disk boundary layer around the hot star. The disk is spatially extended, and cool in its outer regions. The outer extended cool region could have resulted in an eclipse of the Mira variable in 1978. All the jet components A, B, and C2 ejected previously are located inside the opening angle of the ionizing radiation cone (opening angle ~150°). X-rays and UV radiation from the inner hot regions cannot be seen, because the disk is seen nearly edge-on.

of 5×10^{-3} counts s^{-1} obtained with *EXOSAT* by Baratta *et al.* (1985). However, because the observed X-rays are mainly scattered, and the electron-scattering optical depth is small ($\tau_{es}\sim10^{-4}$ in features A and B) the intrinsic X-ray luminosity of the disk could be high, $\sim10^{35}$ ergs s^{-1} ($\sim25\ L_\odot$).

The accretion disk theory of Bath *et al.* (1974), Lynden-Bell and Pringle (1974), and Tylenda (1977) can be used to determine the nature of the hot companion in the system. We find the following relationships for the radius R_2 of the hot star (assumed equal to the inner radius of the accretion disk, r_i); the accretion rate $\dot{M}$ ($M_\odot$ yr^{-1}); the mass of the secondary, M_2; and the disk luminosity L_d ($L_d\sim L_{\rm bl}$), where "bl" refers to the boundary layer:

$$R_2 \gtrsim 5.8\times10^9\left(T_{\rm bl}/10^5\ {\rm K}\right)^{-3/2}\left[N_i/\left(f\times10^{45}\ {\rm s}^{-1}\right)\right]^{1/2}\ {\rm cm}, \quad (10)$$

$$\dot{M}(M_2/M_\odot) \gtrsim 3.2\times10^{-8}\left(T_{\rm bl}/10^5\ {\rm K}\right)^{-1/2} \times\left[N_i/\left(f\times10^{45}\ {\rm s}^{-1}\right)\right]\ M_\odot\ {\rm yr}^{-1}, \quad (11)$$

$$L_d\sim L_{\rm bl}\gtrsim 5.9\left(T_{\rm bl}/10^5\ {\rm K}\right)\left[N_i/\left(f\times10^{45}\ {\rm s}^{-1}\right)\right]\ L_\odot. \quad (12)$$

In relations (10)–(12), the "greater than" sign applies if the observed H II region(s) is (are) photoionized by an accretion disk, with a boundary-layer temperature $T_{\rm bl}$, and the region(s) is (are) density-bound. Otherwise, the equality sign applies, and the H II regions are ionization-bound. N_i is the number of Lyman continuum photons emitted per second, and the parameter f can be found from blackbody tables and has values $f=0.186$, 0.7, and 0.9, for $T_{\rm bl}=40{,}000$, 100,000, and 200,000 K, respectively. The ionizing photon flux N_i can be obtained from the Strömgren theory, and applied to the ionized components B, A, and C2, as well as the central H II region C1. The Strömgren theory should also be applied to the outer extended meniscus-shaped nebula ($r\approx40''$, $n_e\gtrsim100$ cm^{-3}; cf. Solf and Ulrich 1985). From the nebular parameters of § III, we find that a total number of ionizing photons required to ionize the entire R Aqr nebula, assuming an average nebular temperature $T_e\sim15{,}000$ K, is $N_i\sim7.5\times10^{44}$ s^{-1} (cf. Michalitsianos, Kafatos, and Hobbs 1980). We assume that we have ionization-bound conditions, i.e., A, B, C2, and C1, and the outer nebula constitute all of the material involved in photoionization.

Next, we assume that the boundary-layer temperature is in the range $10^5\ {\rm K}\lesssim T_{\rm bl}\lesssim5\times10^5$ K. The lower limit is consistent with N V and He II line emission in component A (and possibly component B; see § III), while the upper limit is determined from the *EXOSAT* observations of Baratta *et al.* (1985). We find that if $T_{\rm bl}=100{,}000$ K, then

$$R_2\sim6\times10^9\ {\rm cm},\quad L_d\sim L_{\rm bl}\sim6.3\ L_\odot,$$

and $\dot{M}\sim3.6\times10^{-8}\ M_\odot$ yr^{-1} (assuming $M_2=1\ M_\odot$). Also, if $T_{\rm bl}=500{,}000$ K, then

$$R_2\sim4.5\times10^8\ {\rm cm},\quad L_d\sim L_{\rm bl}\sim22.2\ L_\odot,$$

$$\dot{M}\sim10^{-8}\ M_\odot\ {\rm yr}^{-1}.$$

Unless the ionizing source is emitting a factor of ~100 more ionizing photons per second compared with the value $N_i\sim7.5\times10^{44}$ s^{-1} which is required to ionize all of the nebular material, the secondary cannot be a main-sequence star. Therefore, it is likely a white dwarf or subdwarf.

The accretion disk becomes geometrically extended in its outer regions during mass transfer. The outer disk radius r_0 is $\sim(1\text{–}2)\times10^{13}$ cm (see Kafatos and Michalitsianos 1982), where the thickness-to-radius ratio is $h/r\sim0.25$, for an outer disk temperature of ~1800 K (Whitelock *et al.* 1983). This extended, cool outer disk can eclipse the Mira variable at periastron, as it seems to have done in the later 1970s. Near the secondary, however, the disk is thin. Thus, for $10^5\lesssim T_{\rm bl}\lesssim5\times10^5$ K, we find $h/r\sim0.001$ in the inner regions. The opening angle of the disk is $\sim150°$ (see Fig. 8), and all the jet components easily fit inside the cone of ionizing radiation. Because the density of the jet components is high, $n_e\sim10^4$ cm^{-3}, the corresponding cooling time scale is $\lesssim1$ yr. The sudden appearance of the jet in the late 1970s is explained in our model as a *sudden increase in the flux of ionizing radiation from the accretion disk, which is accompanied by the photoionization of the jet components*. Furthermore, the position angle of features A, B, and C2 (with respect to C1) suggests that the cone may be precessing. This point will be discussed further in another paper (Hollis *et al.* 1986).

Owing to the radiative cooling time, a photoionized gas parcel will emit UV radiation on a time scale comparable to that of the accretion disk. Accretion from the outer regions of the disk is characterized by a time scale given by

$$t\sim t_r\sim\alpha^{-1}3.3\times10^7\left(M_d/M_\odot\right)^{1/2}\left(r/10^{13}\right)^{1/2}\left(T/10^4\ {\rm K}\right)^{-1}\ {\rm s}, \quad (13)$$

which is $\sim10\alpha^{-1}$ yr; t_r is the drift time scale. Unless $\alpha\sim1$, the disk will last for the entire orbit, which we have assumed is ~44 yr (Willson, Garnavich, and Mattei 1981). The inner disk would only last α^{-1} days, if it were not continuously replenished. We conclude that the outer cool regions of the disk continuously hide the central hot star, but that the ionizing UV flux substantially diminishes, and the X-ray flux completely disappears, when the Mira no longer feeds the accretion disk.

Acceleration of the jet features can be the result of radiation pressure acting on grains. Dust grains would surely not survive in the inner regions of the disk, but should be plentiful in the outer, cool regions of the disk, where $r_0\sim10^{13}$ cm. The opacity of the grains could be as high as 300–1000 cm^2 g^{-1} (Jura and Helfand 1984). Supercritical accretion will, therefore, proceed at rates $\dot{M}\gtrsim\dot{M}_C$, for which

$$\dot{M}_C\sim2\times10^{-8}\left(R_2/10^9\ {\rm cm}\right)\left(\kappa_g/300\ {\rm cm}^2\ {\rm g}^{-1}\right)^{-1}\ M_\odot\ {\rm yr}^{-1}, \quad (14)$$

where κ_g is the opacity due to grains.

We see that equations (11)–(14) give comparable values, which means that a moderate disk luminosity ($L_d\sim10\ L_\odot$; see eq. [12]) can drive the grains away from the outer, cool regions of the disk.

Following Pearce and Mayes (1986), the grain acceleration is given by

$$\ddot{r} = P_r - G_r - D_r, \tag{15}$$

where

$$P_r = 3Q_{\rm pr}L_d/16\pi a_g\rho_g cr^2, \quad G_r = M_2G/r^2,$$

$$D_r = 9\dot{r}n_e(\pi m_{\rm H}kT_e)^{1/2}/4a_g\rho_g. \tag{16}$$

In equation (16), $Q_{\rm pr}$ is the radiation pressure efficiency, which at UV and X-ray wavelengths is ~ 1, and is independent of grain composition (Gilman 1974); a_g and ρ_g are the radius of a grain and the density of grain material, respectively; and n_e and T_e are the gas density and temperature, respectively. Unless $P_r \gtrsim G_r$, there is no acceleration. The minimum grain radius is thus

$$a_g \lesssim 2\times 10^{-5}(Q_{\rm pr}/1)(L_d/L_\odot)$$
$$/(\rho_g/3\ {\rm g\ cm^{-3}})(M_2/M_\odot)\ {\rm cm}.$$

Because $L_d \gtrsim$ a few $L_\odot$, any reasonable grain radius allows acceleration to take place. If $a_g \lesssim 10^5\ {\rm cm^{-3}}$, the first term, P_r, predominates over the second term, G_r. In the absence of negligible drag by gas on the dust grains, i.e., $D_r \ll P_r$, we find that the solution of equation (15) assumes the form

$$\dot{r} = r_0\left[2K/r_0^3(1-r_0/r)\right]^{1/2}, \tag{17}$$

where $K = 3Q_{\rm pr}L_d/16\pi a_g\rho_g c$, and r_0 is the appropriate distance where grain acceleration begins ($r_0 \sim 10^{13}$ cm).

The asymptotic value of expression (17) is $\dot{r} \rightarrow r_0^{-1/2}(2K)^{1/2}$. For values of K of the order of $10^{27}\ {\rm cm^3\ s^{-2}}$ (corresponding to $L_d \sim 10\ L_\odot$, $a_g \sim 2\times 10^{-5}$ cm), we find that $\dot{r} \rightarrow 150(r_0/10^{13}\ {\rm cm})^{-1/2}$ km s^{-1}, which is a fairly low value. The moderate values of ejection velocities observed in the R Aqr nebula (Solf and Ulrich 1985), $v \lesssim 200$ km s^{-1}, are consistent with the grain acceleration mechanism.

Drag on the grains by gas particles will eventually decelerate the grains to a terminal velocity. Equating P_r to D_r in equation (16), we find the following condition:

$$\dot{r}r^2 \sim 1.3\times 10^{36}(n_e/10^4\ {\rm cm^{-3}})^{-1}(T_e/10^4\ {\rm K})^{-1/2}\ {\rm cm^3\ s^{-1}}. \tag{18}$$

Setting an asymptotic velocity of the jet components equal to 50 km s^{-1} (i.e., $\dot{r} = 50$ km s^{-1}; cf. Solf and Ulrich 1985; Wallerstein 1986), we find that $r \sim 5\times 10^{14}$ cm, or $\lesssim 0''.1$, away from the central ionized region. This mechanism naturally explains the low velocities observed in features A and B. Even for feature C2, for which $n_e \sim 4\times 10^5\ {\rm cm^{-3}}$, we find that a terminal velocity of 50 km s^{-1} is achieved at $\sim 10^{14}$ cm separation from the ionizing central H II region. At its present distance ($r \sim 0''.5$) from C1, this feature should be moving with a constant terminal velocity as well.

The accretion disk can form by Roche lobe overflow. Because the binary separation is $a \sim 2.5\times 10^{14}$ cm for a mass of the Mira variable $M_1 \sim 2\ M_\odot$, and a mass of the hot secondary $M_2 \sim 1\ M_\odot$ (Kafatos and Michalitsianos 1982; Wallerstein 1986), the Mira radius $R_1 \sim 300\ R_\odot$ (Kafatos and Michalitsianos 1982) is about one-fifth of the Roche lobe radius. It is for this reason that Kafatos and Michalitsianos (1982) proposed a high eccentricity $e \gtrsim 0.8$ for the orbit. Such an eccentricity would allow the criterion for Roche lobe formation (Haynes, Lerche, and Wright 1980) to be realized, $a(1-e) \sim 2R_1$. Wallerstein's (1986) observations indicate a 44 yr orbit period (see also Willson, Garnavich, and Mattei 1981), with a velocity amplitude of the absorption lines of ~ 7 km s^{-1}, with moderate eccentricity, say $e \sim 0.3$ (G. Wallerstein 1986, private communication). One point, however, in Wallerstein's radial velocity plot does not fit a 44 yr curve. This is the 1965 point, and unfortunately no other points between 1950 and 1970 exist. If the 1965 point is valid, a shorter period and larger eccentricities are possible. Recently, Anandarao, Sahu, and Desai (1985) have analyzed the radial velocity curve of R Aquarii. They have included Johnson's (1980) as well as their own radial velocities computed from the Hα emission-line profile. Anandarao, Sahu, and Desai (1985) conclude that the most probable binary period is about 40–45 yr. Inspection of the figure published in their work indicates that the eccentricity is certainly not zero. It is crucial to obtain accurate radial velocities in the next few years.

Alternatively, the disk may be formed as a result of wind capture. Radio observations imply a mass-loss rate for the Mira of $\sim 10^{-7}\ M_\odot$ yr^{-1} (Hollis *et al.* 1985). The disk requires an accretion rate $\dot{M} \sim 10^{-8}\ M_\odot$ yr^{-1}, implying that the secondary captures $\sim 10\%$ of the wind lost by the Mira. This rate of capture may be hard to realize in a widely separated, circular 44 yr orbit. Even more important, a circular orbit with wind capture does not explain the episodic outbursts and ejections of the various jet components, which seem to happen at intervals that are multiples of the binary orbit (see discussion above). Therefore, we favor an orbit of moderate eccentricity (say, $e \lesssim 0.5$). Future, long-term radial velocity observations are extremely important to determine the orbital characteristics of the binary system. It may be that even with moderate eccentricities, the Mira loses mass to the secondary at appreciable rates, feeding an accretion disk which forms a hot inner region, when the stars are close to each other. The calculations of Haynes, Lerche, and Wright (1980) assume a static primary star. However, when the stars approach each other in a moderately elliptical orbit, say within $\sim 10^{14}$ cm, the radiation from the disk could enhance the mass-loss rate in the hemisphere of the Mira that is exposed to the ionizing radiation field of the disk. This could increase the accretion rate onto the secondary. A similar model has been proposed for compact X-ray sources.

Finally, the properties exhibited by the jet features can be understood if each parcel thermally expands while being slowly accelerated. Because the temperature of the jet components is $\sim 15{,}000$ K, a constant thermal expansion would imply that the size L of each component is proportional to the time each parcel has been moving. Because features A, B,

and C2 parcels move at a constant terminal velocity v, this time is r/v, i.e., $L \propto r$, consistent with observations. A constant column density (see relations [4]) would imply that a particular grain opacity is favored for this mechanism.

V. CONCLUSIONS

Long-term *IUE* observations of the R Aqr jet indicate the following:

1. There is a recent increase in the excitation state of the jet, as evidenced by the strengthening of N V, He II emission and the detection of soft X-rays.
2. The UV line emission from components A and B appears variable on a time scale of ~ 1.5 yr.
3. The various jet components have densities and sizes obeying equations (4).
4. UV observations indicate that the temperature of jet components A and B is increasing.
5. All jet components were ejected at time intervals which are roughly multiples of the binary 44 yr period.

The properties listed above can be understood by the model presented here. An accretion disk forms around the hot secondary. Ionization is provided by the hot, inner regions of the disk, although the disk is extended and cool in its outer regions. Ejection of the gas parcels takes place probably near periastron, in an orbit with moderate eccentricities. Radiation pressure on grains can easily explain the kinematics of the discrete parcels that comprise the R Aqr jet, for luminosities $L \sim 10\ L_{\odot}$. The low expansion velocities which characterize the R Aqr nebula as a whole can be understood if radiation pressure acting on grains is responsible for the ejection process. The jet components remain visible in high-excitation UV emission lines and soft X-rays by scattering, as long as they remain within the ionizing cone of radiation formed by the thick accretion disk. Eventually, as both stars separate, we expect the UV and X-ray radiation to weaken, as the jet components become progressively faint in the optical. Figure 8, which summarizes our model, refers to the system near periastron and near eclipse. Future radial velocity observations, both at visible and at UV wavelengths, should be carried out over extended periods, owing to the long 44 yr binary orbit. We suspect that feature A was ejected during the enhanced activity in the late 1920s, and component C2 corresponds to the most recent ejection event, having been expelled in the mid-1970s.

Finally, Kafatos and Michalitsianos (1982) proposed that the ejection of the outer extended meniscus east-west nebula may have been recorded in historical records of the Far East. From the low densities prevalent in the outer nebula, we estimate a kinetic energy of the outer east-west nebula in the range $\sim 2\times10^{44}$–10^{45} ergs, characteristic of novae and slow novae. Recently, Li (1985) proposed that the "guest star" of A.D. 1073 recorded in the *History of Korea* is possibly a description of the outburst in R Aqr that formed its extended outer nebulosity. If this is correct, R Aqr will afford us one more unique result, namely, the first recorded nova (more correctly, slow nova) with a counterpart record in ancient chronicles.

Higher resolution spectra with the Hubble Space Telescope will yield important information concerning the differences in ionization structure between features A and B, and could, in principle, allow independent estimates of T_e in features A and B.

We wish to thank the resident astronomers of *IUE* and Drs. Yoji Kondo and D. West for support. We also wish to thank Dr. Roberto Viotti for useful discussions concerning his X-ray observations, as well as Dr. Richard Mushotzky for helpful discussions concerning *EXOSAT* data. Support for M. K. was provided by NASA contract NAS5-28721.

REFERENCES

Anandarao, B. G., Sahu, K. C., and Desai, J. N. 1985, *Space Sci.*, **114**, 351.
Baade, W. A. 1944, *Ann. Rept. Dir. Mt. Wilson Obs. 1943–44*, No. 17.
Baratta, G. B., Piro, L., Viotti, R., Cassatella, A., Altamore, A., Ricciardi, O., and Friedjung, M. 1985, in *ESA Workshop on a Cosmic X-Ray Mission* (Lyngby).
Bath, G. T., Evans, W. D., Papaloizou, J., and Pringle, J. E. 1974, *M.N.R.A.S.*, **169**, 447.
Bridle, A. H., and Perley, R. A. 1984, *Ann. Rev. Astr. Ap.*, **22**, 319.
Cameron, A. G. W. 1973, *Space Sci. Rev.*, **15**, 121.
Gilman, R. C. 1974, *Ap. J. Suppl.*, **218**, 397.
Hayes, M. A., and Nussbaumer, H. 1984, *Astr. Ap.*, **13**, 193.
Haynes, R. F., Lerche, I., and Wright, A. E. 1980, *Astr. Ap.*, **81**, 83.
Herbig, G. 1980, *IAU Circ.*, No. 3535.
Hollis, J. M., Kafatos, M., Michalitsianos, A. G., and McAlister, H. A. 1985, *Ap. J.*, **289**, 765.
Hollis, J. M., Michalitsianos, A. G., Kafatos, M., Wright, M., and Welch, W. J. 1986, *Ap. J. (Letters)*, **309**, L53.
Johnson, H. M. 1980, *Ap. J.*, **237**, 840.
_____. 1981, *Ap. J.*, **244**, 552.
_____. 1982, *Ap. J.*, **253**, 224.
Jordan, C. 1969, *Ap. J.*, **156**, 49.
Jura, M., and Helfand, D. J. 1984, *Ap. J.*, **287**, 785.
Kafatos, M. 1973, *Ap. J.*, **182**, 433.
Kafatos, M., Hollis, J. M., and Michalitsianos, A. G. 1983, *Ap. J. (Letters)*, **267**, L103.
Kafatos, M., and Michalitsianos, A. G. 1982, *Nature*, **298**, 540.
Kafatos, M., Michalitsianos, A. G., and Fahey, R. P. 1985, *Ap. J. Suppl.*, **59**, 785.
Kafatos, M., Michalitsianos, A. G., and Feibelman, W. A. 1982, *Ap. J.*, **257**, 204.
Kafatos, M., Michalitsianos, A. G., and Hobbs, R. W. 1980, *Ap. J.*, **240**, 114.
Kaler, J. B. 1981, *Ap. J.*, **245**, 568.
Li, J. 1985, *Chinese Astr. Ap.*, **9**, 322.
Lynden-Bell, D., and Pringle, J. E. 1974, *M.N.R.A.S.*, **168**, 603.
Mauron, N., Nieto, J. L., Picat, J. P., Lelievre, G., and Sol, H. 1985, *Astr. Ap.*, **142**, 413.
Michalitsianos, A. G. 1984, *Comm. Ap.*, **10**, 85.
Michalitsianos, A. G., Hollis, J. M., and Kafatos, M. 1986, *Canadian J. Phys.*, **64**, 85.
Michalitsianos, A. G., and Kafatos, M. 1982, *Ap. J. (Letters)*, **262**, L47.
Michalitsianos, A. G., Kafatos, M., and Hobbs, R. M. 1980, *Ap. J.*, **237**, 506.
Nussbaumer, H. 1986, *Astr. Ap.*, in press.
Nussbaumer, H., and Schild, H. 1979, *Astr. Ap.*, **75**, L17.
_____. 1981, *Astr. Ap.*, **101**, 118.
Osterbrock, D. E. 1974, *Astrophysics of Gaseous Nebulae* (San Francisco: Freeman).
Pearce, G., and Mayes, A. J. 1986, *Astr. Ap.*, **155**, 291.
Penston, M. H., *et al.* 1983, *M.N.R.A.S.*, **202**, 833.
Seaquist, E. R., Taylor, A. R., and Button, S. S. 1984, *Ap. J.*, **284**, 202.
Shull, J. M., Snow, T. P., and York, D. G. 1981, *Ap. J.*, **246**, 553.
Sol, H. 1983, *ESO Messenger*, No. 32, p. 37.
Solf, J., and Ulrich, H. 1985, *Astr. Ap.*, **148**, 274.
Sonnenborn, G. 1984, *IUE Newsletter*, No. 24, p. 67.
Sopka, R. J., Herbig, G., Kafatos, M., and Michalitsianos, A. G. 1982, *Ap. J. (Letters)*, **258**, L32.

Spergel, D. N., Giuliani, J. L., Jr., and Knapp, G. R. 1983, *Ap. J.*, **275**, 330.
Spitzer, L., Jr. 1978, *Physical Processes in the Interstellar Medium* (New York: Wiley).
Taylor, A. R., Seaquist, E. R., and Mattei, J. A. 1986, *Nature*, **319**, 38.
Tylenda, R. 1977, *Acta Astr.*, **27**, 235.
Wallerstein, G. 1986, *Pub. A.S.P.*, **98**, 118.
Wallerstein, G., and Greenstein, J. L. 1980, *Pub. A.S.P.*, **92**, 275.
Whitelock, P. A., Feast, M. W., Catchpole, R. M., Carter, B. S., and Roberts, G. 1983, *M.N.R.A.S.*, **203**, 351.
Willson, L. A., Garnavich, P., and Mattei, J. 1981, *Inf. Bull. Var. Stars*, Nos. 1961–1963.
Wright, A. E., and Barlow, M. J. 1975, *M.N.R.A.S.*, **170**, 41.

J. M. Hollis and A. G. Michalitsianos: Laboratory for Astronomy and Solar Physics, Code 684, NASA/Goddard Space Flight Center, Greenbelt, MD 20771

M. Kafatos: Department of Physics, George Mason University, Fairfax, VA 22030